EFFECT OF CRYOTREATMENT ON THE MICROSTRUCTURAL EVOLUTION OF Ti-Al-Ni-Cr-Co-Fe BASED HIGH ENTROPY ALLOY

A PROJECT REPORT

submitted by

ARJUN SANTHOSH

TKM21MECI05

to

the APJ Abdul Kalam Technological University

in partial fulfillment of the requirements for the award of the Degree

of

Master of Technology

In

Computer Integrated Manufacturing

Department of Mechanical Engineering

TKM College of Engineering

Kollam

JULY 2023

DECLARATION

I, **ARJUN SANTHOSH** hereby declare that the project report **"EFFECT OF CRYOTREATMENT ON THE MICROSTRUCTURAL EVOLUTION OF Ti-Al-Ni-Cr-Co-Fe BASED HIGH ENTROPY ALLOY**." submitted for partial fulfillment of the requirements for the award of degree of Master of Technology of the APJ Abdul Kalam Technological University, Kerala is a bonafide work done by me under supervision of **DR.ANAND SEKHAR R**, Assistant Professor, Department of Mechanical Engineering, TKM College of Engineering, Kollam. This submission represents my ideas in my own words and where ideas or words of others have been included, I have adequately and accurately cited and referenced the original sources. I also declare that I have adhered to ethics of academic honesty and integrity and have not misrepresented or fabricated any data or idea or fact or source in my submission. I understand that any violation of the above will be a cause for disciplinary action by the institute and/or the University and can also evoke penal action from the sources which have thus not been properly cited or from whom proper permission has not been obtained. This report has not been previously formed the basis for the award of any degree, diploma or similar title of any other University.

Signature:

Name of the Student: **Arjun Santhosh**

Register No: **TKM21MECI05**

KOLLAM

Date: 07/07/2023

DEPARTMENT OF MECHANICAL ENGINEERING
TKM COLLEGE OF ENGINEERING, KOLLAM

CERTIFICATE

This is to certify that the report entitled **'EFFECT OF CRYOTREATMENT ON THE MICROSTRUCTURAL EVOLUTION OF Ti-Al-Ni-Cr-Co-Fe BASED HIGH ENTROPY ALLOY'** submitted by **'ARJUNSANTHOSH (TKM21MECI05)'** to the APJ Abdul Kalam Technological University in partial fulfillment of the requirements for the award of the Degree of Master of Technology in Computer Integrated Manufacturing, Mechanical Engineering is a bonafide record of the project work carried out by him under my guidance and supervision. This report in any form has not been submitted to any other University or Institute for any purpose.

18/7/23

Internal Supervisor:
Dr. Anand Sekhar R
Assistant Professor
Department of Mechanical Engineering
TKM College of Engineering, Kollam-5

PG Coordinator: **Kannan. S**
Assistant Professor
Dept. of Mechanical Engineering
TKM College of Engineering,
Kollam-5

Dr. P.N. Dileep
Head of the department,
Department of Mechanical Engineering
TKM College of Engineering, Kollam

ACKNOWLEDGEMENT

First of all, I am indebted to the **GOD ALMIGHTY** for giving me an opportunity to excel in my efforts to complete this project on time.

I am extremely grateful to **Dr. T SHAHUL HAMEED**, Principal, TKM college of Engineering and **Dr. P.N. DILEEP** , Head of the Department, Department of Mechanical Engineering, for providing all required resources for successful completion of my project.

I am greatly obliged to my internal supervisor **Dr.ANAND SEKHAR R**, Assistant professor, Department of Mechanical Engineering, for his encouragement, guidance and support.

My heartfelt gratitude to **Prof. KANNAN S.**, PG coordinator, Department of CIM & **Prof. FAIZAL N. S.**, Assistant professor, Department of CIM for their valuable suggestions and guidance in the preparation of the project presentation and report.

I express my thanks to all Faculties and Technical staffs, Department of Mechanical Engineering, and all staff members and friends for all help and coordination extended in bringing out this project successfully in time.

I will be failing in duty if I do not acknowledge with grateful thanks to the authors of the references and other literatures referred to in this project.

Last but not the least, I am very much thankful to my parents who guided me in every steps which I took.

Place: KOLLAM **ARJUN SANTHOSH**

Date: 07/07/2023

ABSTRACT

High Entropy Alloys (HEAs) are new class of materials. Recent Studies on HEAs have attracted much attention in the field of scientific research and industry. There has been a lot of interest in HEA compositions having a BCC structure. However, analysis of deep cryotreated Ti-Al-Ni-Cr-Co-Fe-based alloys on the structure and mechanical behavior of these BCC HEAs has not been performed so far. This project aims to determine the impact of deep cryogenic treatment on those factors by investigating the phase composition, microstructure, and characteristics of the TiAlNiCrFe and TiAlNiCrCo high-entropy alloys. Through the ball milling of elemental powders and Spark Plasma Sintering, multicomponent alloys of TiAlNiCrFe and TiAlNiCrCo were effectively created. XRD patterns showed that both materials had substantial two-BCC phases after Spark plasma sintering. In the TiAlNiCrFe and TiAlNiCrCo samples, SEM BSE images of the microstructure samples showed a fine dispersion of the two BCC phases coupled with a fine dispersion of TiC nanoparticles. The impact of deep cryogenic treatment on the phase composition, crystallite sizes, microstructure, and mechanical characteristics of TiAlNiCrFe and TiAlNiCrCo high-entropy alloys were successfully investigated. The XRD patterns say that the 4 and 8-hour treated TiAlNiCrFe and TiAlNiCrCo samples show major BCC peaks similar to as-sintered alloys, and small TiNI3 peaks are also present in both 4,8-hour treated alloys. Hardness seemed to rise initially before decreasing as the duration of the cryogenic treatment increased. At 4-hourly treated samples have finer crystallite sizes and maximum hardness was attained. The hardness value of TiAlNiCrFe alloy after 4-hour treatment rises from 755 HV to 840 HV by 11.25%.

Keywords: High Entropy Alloys, Cryogenic treatment, Spark Plasma Sintering.

CONTENTS

LIST OF FIGURES

LIST OF TABLES

ABBREVIATIONS

BCC	Body centered cubic
CT	Cryotreatment
DCT	Deep cryotreatment
EDM	Electrical discharge machining
EDS	Energy dispersive spectroscopy
EPAC	Electric pulse assisted consolidation
FAST	Field assisted sintering technology
FCC	Face centered cubic
HCP	Hexagonal closed pack
IMs	Inter metallic compounds
PECS	Pulsed electric current sintering
SEM	Scanning electron microscope
SPS	Spark plasma sintering
TEM	Transmission electron microscope
W-H	Williamson Hall plot
XRD	X-ray diffraction

CHAPTER 1

INTRODUCTION

A metallic material known as an alloy is made up of two or more elements, either as a compound or a solution. Conventional alloys have traditionally been based on one or two main constituents, such as nickel and cobalt for super alloys and iron for steel alloys. High entropy alloys (HEAs) can be categorized under two main headings. According to the first definition that was given to them, high entropy alloys are a novel class of metallic systems that contain at least five different principle elements. principle elements are defined as those that make up at least 5% of an alloy's composition. Their projected level of mixing entropy was utilized as the basis for the second definition that was used to define them. The entropy of mixture is another definition that has been used to distinguish the idea of high entropy alloys. According to this definition, a high entropy alloy is any alloy that possesses a configurational entropy greater than 1.5R. Several elements were blended to create an alloy which was able to supply and improve specific properties as required for the application due to the constraints of using pure metals [1].

Over the course of a thousand years, the idea of creating alloys has changed. Additionally, an entirely novel strategy to alloy creation known as high entropy alloy (HEA) was uncovered in the early decades. To create fresh material, a number of key features are being implemented with great focus. The researchers are revealing a number of previously unknown characteristics of the multi-dimension composition space. Nevertheless, a sizable number of properties have been found. Despite this, due to their low melting temperatures, alloys based on intermetallic compounds have been developed as high-temperature materials having the main objective of replacing nickel-based superalloys [2]. These alloys are constantly being produced since there is still a lot of interest in applications in delicate situations. Alloys used in high-temperature applications must possess mechanical strength, microstructural stability, and resistance to corrosion and oxidation. The main materials employed in high-temperature environments and the hot sections of aircraft turbine engines may be high entropy alloys.

High-entropy alloys (HEAs) are these alloys with unusually high mixing entropy that frequently exhibit straightforward solid-solution geometries like face-centered cubic (FCC), body-centered cubic (BCC), and close packed hexagonal (HCP). High-entropy multicomponent systems Cantor alloys are face-centered cubic single-phase or nearly single-

phase alloys that take up a significant amount of multicomponent phase space. Because of its exceptional ductility and fracture toughness, which set the Cantor alloy apart as a high-entropy alloy, it has become one of the most promising alloy systems in the last fifteen years. The Cantor alloy's low strength, however, has significant limitations on its technical uses.

Both at low temperatures and at high temperatures, HEA compositions exhibit robust mechanical properties. Deep cryogenic treatment, a form of heat treatment, is widely used to study conventional alloys. It is also clear that conventional alloys can function more effectively following significant cryogenic treatment [4-5]. Contrary to casting, which produces more homogenous microstructures and has the benefit of creating nano-crystalline and metastable microstructures, mechanical alloying produces more homogeneous microstructures than the majority of HEAs reported in the literature. Vacuum hot pressing, mechanical alloying, and other processing procedures were used to these alloys [6-8]. A nanocrystalline microstructure with crystallite diameters under 10 nm is also seen in these alloys after 6 hours of milling. In the present investigation, HEAs with nominal TiAlNiCrFe and TiAlNiCrCo compositions were mechanically alloyed prior to being sintered using Spark Plasma Sintering (SPS). The phase composition, microstructure, and alloy characteristics were examined before and after deep cryogenic treatment, which was applied for a variety of times.

1.1 HISTORICAL DEVELOPMENT OF ALLOYS

The creation of new materials has a significant impact on human civilization. Stone, wood, leather, bone, and indigenous metals like gold, silver, and copper were among the natural materials used by early humans throughout the Stone Age. Ceramics, polymers, and metals are the three main types of materials that are covered under these materials. Because it was simpler to reduce copper, tin, lead, mercury, and iron from their respective ores after the Stone Age, following ages (i.e., Bronze, Iron, and Steel) followed one after the other. As a result, the technology to create these materials in vast quantities was developed. Steels, cast iron, and copper alloys were produced by alloying iron primarily with carbon from combustion fuels and by alloying copper mostly with tin and lead. When compared to the old ceramics and polymers, the majority provide higher strength and toughness combinations. These produced effective uses for daily tasks, transportation, building, and weaponry.

Due to weak deposits or extremely challenging reduction and extraction processes, the identification of new metal elements was sluggish. But following the First Industrial

Revolution, which got underway in England about 1750, substantial advancements were made. As new elements were discovered and produced using a variety of processes, new alloys were gradually created and used in both routine and unique applications. This led to quick developments. A total of 30 alloy systems were created and commercialized, each based on a different primary metal element. High-speed steels, stainless steels, aluminium alloys, alnico alloys, Cu-Be alloys, super alloys, and titanium alloys are a few popular industrial alloys. Ni-Al, Ti-Al, and Fe-Al intermetallic compounds and alloys [8], as well as metallic glasses for specialized applications, are examples of recently created alloys from the middle of the 20th century.

1.2 MULTICOMPONENT ALLOYS: A CONCEPTUAL FRAMEWORK

Traditionally, one main element or compound has been used almost exclusively in the production of native metals and synthetic alloys from extractive elements. While alloying metals enhances certain mechanical, physical, or chemical qualities for specific purposes, pure metal elements with low impurities are still employed in electrical, jewelry, optical, and other unique applications. The majority of useful alloys are composed of many components. The goal of metallurgists was to create new alloys by combining many metal components in huge quantities. This approach is discouraged, though, as melting and casting the metals need a high temperature and the cast alloys frequently turn brittle and hard. Possibly the only scholar identified in literature as having examined multicomponent equi-mass alloys is Franz Karl Archard, a German physicist and metallurgist who lived in the late eighteenth century. His findings demonstrated that the qualities of the alloys are varied but unappealing, using five to seven elements chosen from the eight commonly occurring elements at the period, including iron, copper, tin, lead, zinc, bismuth, antimony, and arsenic. It is obvious that this is the reason why ancient civilizations did not realize alloys with numerous primary alloying elements in high amounts.

Physical metallurgy and materials science still discourage the study and creation of multicomponent alloys that are not based on a single primary element or single compound. Binary or ternary phase diagram-based information reinforces this reality. The majority of phase diagrams display either intermetallic compounds (IMs), which are ordered structures with compositions in stoichiometric ratio or near-stoichiometric ratio, or intermediate phases (IPs), which are compound-type solid solutions with relatively wide composition ranges and are also known as intermetallic phases. Except in cases where one or more variables are fixed,

quaternary phase diagrams cannot exist in three dimensions. Nevertheless, given the rising tendency from binary to ternary systems, it is anticipated that quaternary phase diagrams will contain a greater number of equilibrium IMs or IPs. In addition, alloys with additional alloying components frequently have more equilibrium or nonequilibrium IMs or IPs. As a result, the conventional notion continues to rule the design, manufacturing, and use of alloys. Any trial that goes against this idea is often regarded as being irrational and useless. Thus, the classic alloying idea still places limitations on the possibilities of discovering unique microstructures, characteristics, and applications. Without a full grasp of alloys containing numerous major elements, alloy information relating to materials science, engineering, and solid-state physics would be incomplete.

1.3 HIGH-ENTROPY ALLOYS OVERVIEW

Depending on how well humans were able to develop the materials, alloys progressed from simple to complex compositions. The enhanced functions and performances of alloys that result allow for civilizational development. Special alloys including superalloys, stainless steels, and high-speed steels were created in the previous century as a result of tremendous development and advancement. Despite the fact that alloys made of many different elements have greater mixing entropies than pure metals, the increased qualities are mostly the result of higher mixing enthalpies, which enable the inclusion of suitable alloying elements to boost strength and enhance physical and/or chemical properties. More complicated compositions with greater mixing entropies have been made available since the turn of the century. Such complex compositions do not always imply complex structure and microstructure or the brittleness that goes along with them. On the other hand, greatly increased mixing entropy resulting from complicated compositions might simplify the structure and microstructure and provide the alloys desirable qualities. High-entropy alloys and equi-atomic multicomponent alloys were independently proclaimed as feasible in publications released in 2004 by Jien-Wei Yeh and Brian Cantor. Over the last eighteen years, research on these novel materials has spread over the globe due to this major development in alloying principles.

CHAPTER 2

BACKGROUND STUDY

Since the beginning of time, pure metal has been on a path towards alloys and superalloys that are essential for creating new metallic materials. The high thermal strength of the nickel-based superalloy, which is frequently utilized in turbine components, is its main selling point. Superalloys based on nickel typically have a monocrystalline form [1]. The Ni-base superalloy contains all the characteristics that might be used to make engine components. Due to the alloy's unfortunate initial melting point of roughly 1300^0C, its operating range has been restricted to 1160^0C to 1277^0C. Additionally, lower density elements like aluminium (Al), magnesium (Mg), beryllium (Be), and titanium (Ti) could be used for high-temperature applications. However, the main challenge in synthesizing HEAs containing lower density elements has their higher reactivity with an environment, effectively lower melting point, and cost-efficiency. However, Ti is strong structural qualities make it a popular choice for high-temperature applications. One often used to mean of the term "high temperature" in materials science and technology is "a temperature equal to, or greater than, approximately two-thirds of the melting point of a solid" [2-4].

A novel class of alloy was created by Cantor and Yeh et al. in 200 based on the maximization of configuration entropy and formation of a stable, single phase, substitutional solid solution. The alloy is also known as a multi-component alloy, multi-principal alloy, or complicated concentration alloy since it has five or more elements with a concentration of between 5 and 35 at%. The configuration entropy is not the only factor that influences the creation of solid solutions [5]. Several investigations have shown that the production of several different phases and the compound occurs often. In a certain range of compositions of alloying elements, the single-phase solid solution formation has been observed. It is interesting that the determination of phase stability has mostly depended on enthalpy and non-configurational entropy [6-7].

Thermal study, however, has shown that configurational entropy is the major driver behind the formation of the single-phase. Numerous variable characteristics, including as the melting temperature, processing temperature, interatomic correlation, and specific elemental properties that are present in the alloy system, may have an impact on the development of the random solid solution [8-12]. High entropy alloys (HEAs) are receiving more attention from materials scientists all around the world because of their unique structures and characteristics. The first

concept placed a major emphasis on maximizing mixing entropy to generate straightforward substitutional solid solutions. Certain multi-component equiatomic alloys which have a remarkably stable single substitutional solid solution structure were identified, despite it subsequently being shown that the mixing entropy has a minor impact on the phase selection for these alloys. The Cantor (CoCrFeMnNi) alloy, which has a reliable face-centered cubic (FCC) structure, is the most well-known example. Some of these HEAs have also shown some highly desirable qualities [11-13]. For instance, certain alloys made of refractory elements have great high temperature strength, whereas the Cantor alloy and its variants offer excellent fracture toughness at a cryogenic temperature. The reduction in the stacking fault energy as the deformation temperature drops can be used to explain the higher dislocation density and nano-twins at cryogenic temperatures. These researches may offer a thorough knowledge of the mechanisms that keep HEAs strong under various temperature circumstances and may serve as a roadmap for discovering HEAs with exceptional mechanical characteristics in cryogenic environments. Nonferrous metals such alloys of aluminium (Al), copper (Cu), and magnesium (Mg) can also be treated using deep cryogenic treatment [2,4,12]. It is clear that deep cryogenic treatment can enhance the performance of conventional alloys; however, prior research has mostly concentrated on conventional alloys, and no proposal for an examination into the impact of deep cryogenic treatment on high-entropy alloys has been made. Ti-Al-Ni-Co-Cr-Fe based alloy was subjected to deep cryogenic treatment for varying lengths of time, and the phase composition, microstructure, and properties of the alloy before and after treatment were studied. This was done to determine whether cryogenic treatment has a similar impact on the performance of HEAs.

CHAPTER 3

LITERATURE REVIEW

Currently, there is a lot of research interest in high-entropy alloys (HEAs) in materials science and engineering. Novel characteristics of HEAs, including as their outstanding specific strength, improved mechanical performance at high temperatures, extraordinary ductility and fracture toughness at cryogenic temperatures, super Para magnetism, and superconductivity, are also highlighted. This literature review aims to provide an overview of recent developments in the field of HEAs. Here is a brief literature review of some of these studies.

Cantor and I.T.H. Chang et al. [1] describes an initial attempt to investigate the unexplored central region of multicomponent alloy phase space. In their experiment 20 elements were included in the first alloy under investigation in identical atomic quantities, i.e., 5 at.% of each of the following elements: Mn, Cr, Fe, Co, Ni, Cu, Ag, W, Mo, Nb, Al, Cd, Sn, Pb, Bi, Zn, Ge, Si, Sb, and Mg. The second alloy included the same 16 elements as the previous one, with the exception of the semi-metals Bi, Ge, Si, and Sb, and had 6.25 at.% of each of Mn, Cr, Fe, Co, Ni, Cu, Ag, W, Mo, Nb, Al, Cd, Sn, Pb, Zn, and Mg. Both alloys shows multiphase structure with brittle character. The microstructures and characteristics are then investigated using multiple techniques of optical microscopy, scanning electron microscopy, and electron probe microanalysis. Cantor et al. find that both as-cast and after melt spinning, alloys with equal amounts of 16 and 20 components are multiphase, crystalline, and brittle. A single FCC solid solution made up of the five components of the alloy Fe20Cr20Mn20Ni20Co20 and it solidifies dendritically.

Chengze Li et al. [2] evaluated the effects of deep cryogenic treatment on the microstructure and characteristics of AlCrFe2Ni2 high entropy alloy by analyzing the phase composition, microstructure, and properties following cryogenic treatment. They discovered that deep cryogenic treatment significantly enhanced the alloy's hardness, yield strength, and wear resistance. Face-centered cubic (FCC) and body-centered cubic (BCC) phases formed by the alloy. The band FCC phase structures got shorter and more disordered as the treatment period increased, and the grain orientation of the BCC phase and B2 phase shifted and transitioned into one another. With a holding period of 4 hours, the alloy performed at its best, and its Vickers hardness (338 HV) was 11.6% greater compared to its as-cast counterpart.

Vikas Kukshal et al. [3] investigate the effect of Co addition on AlCr1.5CuFeNi2Cox high-entropy and X-ray diffraction (XRD), scanning electron microscopes (SEM), Vickers microhardness testers, and Universal Testing machines were used to investigate the materials' microstructure, phase change, density, microhardness, and compressive strength. Vikas Kukshal et al, finds that the alloys' crystalline structure displays simple FCC and BCC phases. The microstructure analysis of the alloys reveals that the Cu-rich FCC phase is the consequence of segregation of copper in the interdendrite region. The micro hardness value of the alloys decreases from 471 HV to 364 HV with an increase in the cobalt concentration from x = 0 to x = 1 (molar ratio), as the inclusion of Co further promotes the development of the FCC phase. The alloy's compressive strength shows a similar trend of declining strength [3].

Klimova et al. [4], conducted experimental study on HEAs and They looked at the equiatomic CoCrFeMnNi alloy's microstructure and tensile characteristics at both room temperature and cryogenic temperatures with the addition of N in different amounts. Investigations were also done on the alloy's microstructures following tensile testing. They resulted a single FCC phase with a coarse-grained microstructure was seen in the alloys with low amounts of N (0.5–1.0 at. %). A small quantity (less than 1%) of Cr-rich M2N nitride particles precipitated when the N content was raised to 2.0 at.%. The yield strength of the alloys increased according to the N % [4].

Wujing Fu et al. [5] Studies give a thorough grasp of the mechanisms that enhance HEAs under various temperature settings and direct research towards HEAs with exceptional mechanical characteristics in cryogenic environments. According to Wujing Fu et al, the lattice structure of CrMnFeCoNi HEA deviates significantly from the original crystal structure during elastic deformation below room temperature, indicating that the lattice structure underwent significant deformation before plastic deformation. Dislocation density is also higher at cryogenic temperatures than at room temperatures. Large crystallographic distortion can boost Peierls-barrier stress and prevent dislocation nucleation, increasing the yield strength of the HEA at cryogenic temperatures.

Daniel Costas Bosque et al. [6], study the effect of Al addition to the high entropy system HfMoTaTi+Al. Through the SPS approach, a high entropy HfMoTaTiAl alloy was created and studied. It was demonstrated using XRD that the system was structured according to a BCC model. The system's characteristics were enhanced by the addition of aluminium; density was lowered by 17%, and hardness rose by 6% to 15%.

W.H. Liu et al. [7], fabricate a six component HEAs and examine the alloying impact of Al on the structure and tensile characteristics, for instance, the as-cast structure in the $Al_xCoCrFeNiTi$ system tends to change as the Al concentration rises from a combination of FCC + BCC duplex phases to a single bcc phase. Transmission electron microscopy was used to analyse the microstructures of these alloys, and crystalline phase progression was described and compared with XRD. According to W.H. Liu et al., alloys with an Al content of less than 8% behave like solid solution alloys and use the additional Al atom as their main fortifier. Alloys have an elongation range between 61.7% and 47.2%, a yield strength of 220 MPa, and a tensile strength of 500 MPa. Aluminium concentrations between 8% and 16% demonstrate the emergence of bcc phases, as well as a strong rise in fracture and yield strength, but a dramatic decrease in ductility. In this area, alloys act like composites. Alloys with an Al content of more above 16% have disordered A2 precipitates encased in an ordered B2 matrix. It is suggested by microstructural analysis that the two bcc phases developed.

R. Anand Sekhar et al. [8] conducted and experimental study and TiAlNiCo, TiAlNiFe and TiAlNiCoFe HEAs' are manufactured through mechanical alloying followed by Spark Plasma Sintering (SPS), and the effects of composition on their microstructure and mechanical characteristics were investigated. R. Anand Sekhar et al find that After 8 hours of milling, homogeneous mixing and the development of the BCC phase were noted. The two BCC phases and TiC nanoparticles were finely dispersed after SPS, according to the microstructure's SEM results. Comparing the TiAlNiCoFe alloy to the 4-component alloy, extremely few TiC nanoparticles were present, suggesting a sluggish development rate caused by slow diffusion. Vickers indenter measurements of the alloys' hardness also yield positive results, with values around 700 HV.

Sajid Ali Alvi [9] fabricated a CuMoTaWV HEA that was made via SPS revealed a composite structure with the development of the BCC HEA phase and the existence of the hard V-rich phase. This research assisted us in demonstrating the importance of RHEA's microstructure and elemental choice for tribological applications at various temperatures. Sajid Ali Alvi finds due to the development of tribofilms rich in oxides of W and Ta and the existence of hard V-rich phases, the tribological characteristics demonstrated low frictional and wear qualities at room temperature. At 400^{o}C and 600^{o}C during tribology tests, adaptive wear behavior was

seen. CuO was produced as a result of the oxidation of Cu at 400^{o}C, which helped to decreasing wear.

Amanendra Kushwala et al. [10] developed nanocrystalline pure aluminium powders using cryomilling technique followed by spark plasma sintering (SPS). The cryomilling was performed on pure Al powders for 2, 6 and 8h. Then they investigated the particle morphology and crystallite size of powders by using SEM, XRD techniques and mechanical properties investigated by Vickers micro hardness tester. The results of their study show that crystallite size of pure Al powders decreases with increased cryomilling time and after spark plasma sintering the crystal size is slightly elevated. XRD studies suggest that the reduction in the crystallite size with increasing cryomilling time and after SPS the crystallite size is increases for 8h cryomilled sample.

Liyang Fanga et al. [11], studied the effect of Cr content on microstructure characteristics and mechanical properties of $ZnNbTaHfCr_x$. Vacuum arc melting was used to create a series of $ZrNbTaHf0.2Cr_x$ alloys, designated as Cr0, Cr0.3, Cr0.5, Cr0.75 and Cr1, and the microstructure, phase components, and mechanical characteristics of the refractory high-entropy alloy were investigated. According to Liyang Fanga et al., the alloys create the dendritic region's BCC solid solution phase, the interdendritic region's HCP solid solution phase, and the dendritic region's C15 Laves phase. With an increase in Cr concentration, the lattice parameter of the BCC phase falls and the volume fraction of the Laves phase rises. Nb and Ta are concentrated in the BCC phase, Cr is abundant in the Laves phase, and Zr and Hf are enriched significantly in the HCP phase. The alloy becomes harder and has a higher yield strength, but its density falls. The hardness significantly rises with the addition of the Cr element, rising from 353.9 3.5 HV for the cast Cr0 alloy to 530.9 5 HV for the Cr1 alloy.

Chun-mei Li et al. [12], investigated the mechanical characteristics of the Al-Zn-Mg-Cu alloy and the Deep Cryogenic Treated (DCT) induced phase transition. By using semi-continuous casting, an Al alloy (Al-Zn0.078-Mg0.018-Cu0.015) was created. Step-homogenization of the as-cast samples took place at 430°C for 18 hours and then at 467°C for 4 hours. The DCT method was then used multiple times, along with the conventional solution and anti-aging therapies, at various phases. According to the experimental findings, the DCT time has a significant impact on the sample's hardness. The characteristics of the alloy are improved by the Al matrix while keeping the beneficial discontinuous distribution at grain boundaries with 30–40–nm precipitate-free zones. DCT may change the mechanical characteristics of Al alloys

by optimizing their microstructures, however the hardness does not rise linearly with the increase in DCT time and instead decreases when the DCT period is prolonged.

Srinivasa Rao Bakshi, R. Anand Sekhar [13], investigated at how the Cr additions affected the microstructure of a Ti-Al-Ni (Cr, Co, Fe) alloy. Through mechanical alloying and spark plasma sintering (SPS), they created high entropy alloys of TiAlNiCr, TiAlNiCrCo, TiAlNiCrFe, TiAlNiCrCoFe, and TiAlNiFe. The microstructures of the alloys were analyzed using scanning electron microscopy and energy-dispersive spectroscopy (EDS), and the crystal structures of the powders as-milled and pellets following SPS were examined using an X-ray diffractometer. According to [13], the predominant phase seen in the alloys after milling has been determined to be a BCC phase which is of Cr type in alloys with Cr and Cr, Fe rich in alloys having Fe as well. This is shown by the XRD peaks of alloys with Cr after 8 h of milling and after SPS. After SPS, the second significant peak seen in alloys lack of Cr has been classified as NiAl type. It demonstrates that all alloys produce a single BCC phase following SPS, which can be of the NiAl type or the Fe type, for phase development in alloys lacking Cr. SEM BSE images shows white, gray regions. The two alloys underwent EDS analysis, and the results indicate that the white phase is rich in Cr and Fe whereas the grey phase is rich in Ni and Al. These findings are consistent with the peaks seen in the XRD patterns of all four alloys, which implies that the alloys form a BCC phase. After 8 hours of milling, the alloys all transition into simple solid solution BCC phases. One additional BCC phase is produced as a result of SPS, and as the number of alloying elements rises, so does its peak XRD intensity. Cr-/Cr-Fe-rich BCC 1 phase and NiAl-/Co-rich BCC 2 phases may have formed, according to BSE pictures and EDS.

Zhiyi Ronga et al. [14], created coatings made of the high-entropy alloys FeCoNiCr, FeCoNiCrMn, and FeCoNiCrAl by using electrodeposition in an acidic environment. They then investigated the coatings' microstructure, hardness, wear, and corrosion. By using the X-ray diffraction (XRD) method, the crystal structure and phase of the as-prepared materials were characterized. The XRD patterns of the high-entropy alloy coatings made of FeCoNiCr, FeCoNiCrMn, and FeCoNiCrAl show that all of the elements are dissolved into the same crystal lattice to create a single disordered solid solution phase. In addition, the increased lattice parameters brought on by the difference in atomic size distorts the crystal lattice. According to Zhiyi Ronga et al. [14], the HEA coatings' surfaces are uniform and smooth, and their surface microstructures exhibit a characteristic cell-like structure. Single FCC phase builds up these

coatings on high-entropy alloys. The FeCoNiCrX (Mn, Al) HEA coatings enhance the substrate's microhardness and wear resistance. Because Cr elements are firmly soluble in the coatings' FCC phase and provide a higher lattice distortion effect, which raises the hardness of the FCC phases, the inclusion of Cr elements greatly improves the coatings' hardness.

R. Sriharitha et al. [15] created a multi-component AlxCoCrCuFeNi (x = 0.45, 1, 2.5, and 5 mol) high entropy alloy that was mechanically alloyed, spark plasma sintered to create high dense compacts, and examined its crystallite, microstructural properties using X-ray diffraction and scanning electron microscopy. By annealing the SPS samples at 400, 500, and 600 ^{0}C for 2, 5, and 10 h at each temperature, the thermal stability of Al0.45CoCrCuFeNi and AlCoCrCuFeNi HEAs was examined. Three phase microstructures have been found in SPS samples of Al0.45CoCrCuFeNi and AlCoCrCuFeNi, according to R. Sriharitha et al. The high entropy alloys change from three phase (predominantly FCC-Fe (Ni, Co) with some amount of second FCC-Cu (Ni) and BCC-Cr (Fe, Co) to single phase (B2-NiAl (Fe, Co, Cr)) with increase in Al content. The highest Al content achieved a very high specific hardness of 160 HV/gcm^{-}3. Thermal stability investigations showed that these nanocrystalline high entropy alloys exhibit slow grain development when operated at three distinct temperatures of 400, 500, and 600 ^{0}C for periods of 2, 5, and 10 hours.

S. Varalakshmi et al. [16], created a nanostructured, equiatomic, high entropy solid solutions in the Al-Fe-Ti-Cr-Zn-Cu system from binary to hexanary compositions by mechanical alloying. An energy dispersive X-ray (EDX) microanalysis system with a scanning electron microscope (SEM) was used to evaluate the chemical composition of the ground-up powders. By using a transmission electron microscope (TEM), the milled powders' nanocrystalline makeup and crystal structure were examined. S. Varalakshmi et al. conclude from the findings and analysis that the majority of crystallite sizes after 10 hours of milling are below 10 nm. EDX microanalysis has verified the homogeneity of the chemical composition of all high entropy alloys. The crystallite size estimated from the X-ray peak broadening is extremely similar to the particle size obtained from the TEM research (10 nm).The AlFeTiCrZnCu high entropy alloy was sintered at 800 °C for 1 hour, and the XRD pattern shows that the alloy is a single phase solid solution with a BCC structure and is nanocrystalline (crystallite size of 20 nm) even after sintering, demonstrating the solid solution's high stability and 2 GPa hardness.

3.1 SUMMARY OF LITERATURE REVIEW

The literature review suggests that HEAs are currently the subject of more and more research. The ideal alloy in alloy engineering has a low density and high strength/hardness [1-3]. Numerous investigations revealed that the addition of certain elements to HEAs might have a significant impact on their mechanical characteristics, microstructural morphology, and crystalline structure [3-12]. In instance, CrMnFeCoNi alloy (Cantor alloy), which has outstanding low-temperature ductility, is the FCC-type HEA that has been explored the most. However, there is not much known about how other interstitial materials affect the structure and characteristics of HEAs. BCC-structured HEA compositions have drawn a lot of attention. However, no investigation of the structure and mechanical behavior of this bcc HEAs using deep cryotreated Ti-Al-Ni-Cr-Co-Fe based alloy has been done to yet. The majority of HEAs described in the literature are produced using the casting approach. A thorough study of these microstructures reveals segregations in the interdendritic areas and a typical dendritic microstructure. Mechanical alloying creates more homogenous microstructures than casting and has the benefit of producing nano-crystalline and metastable microstructures [13-16]. Overall, the literature suggests that further research is needed to investigate the microstructural analysis on cryotreated HEAs synthesized through mechanical alloying followed by SPS.

3.2 OBJECTIVES

- To fabricate the HEAs samples through mechanical alloying followed by SPS.
- To characterize the manufactured samples.
- To do cryogenic treatment on these samples.
- To examine the phase and outcomes of the microstructural examination on samples that have undergone cryotreatment, compare the samples' before-and-after data.

3.3 METHODOLOGY

Preparation of elemental powders for mechanical alloying is the first step. Next the synthesized samples undergone mechanical alloying followed by spark plasma sintering. Then the Samples were cut using wire EDM for microstructural research, and the cross section was prepared and polished using emery sheets and diamond cloth. Scanning electron microscopes (SEM) and X-ray diffraction (XRD) were used to characterize the microstructure. After characterization the samples were soaked in liquid nitrogen for 4,8hrs and then allowed to cool to room temperature. SEM and energy-dispersive spectroscopy (EDS) were employed to study the microstructures of the alloys, and X-ray diffraction was utilized to assess the phase structure of the alloys. The Flowchart for the methodology is shown in figure 3.1.

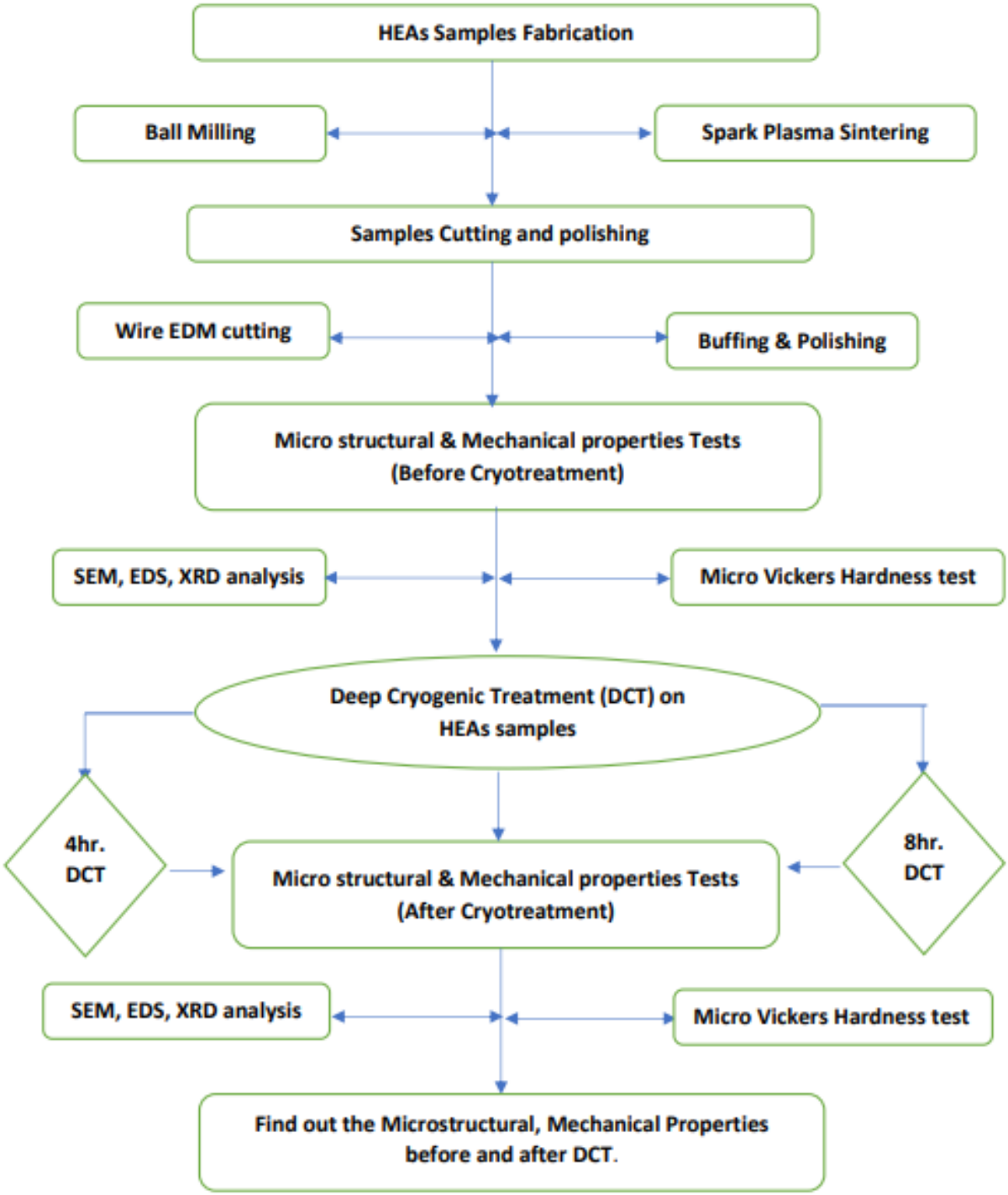

Fig 3.1 Flowchart of Methodology

CHAPTER 4

EXPERIMENTAL SETUP AND PROCEDURE

The following approach was devised for the experiments in order to meet the project's objectives.

4.1 SAMPLES PREPARATION

4.1.1 SELECTION OF ELEMENTS

It has been shown in several experiments that adding aluminium (Al) improves HEA's mechanical characteristics, such as yield strength, Young's modulus, and hardness, even if it decreases fracture strain. The density lowering of the HEA in which aluminium is added is a significant additional component [18]. In comparison to the other elements, Al and Ti are better additives [11]. Titanium is a significant industrial metal that is lighter than steel, stronger than aluminium, and has excellent corrosion resistance. Due to their exceptional biocompatibility, titanium alloys are also employed in medicinal applications. Titanium alloys are frequently used in engines, aero plane frames, maritime equipment, and industrial operations [17]. NI-Al phases show high temperature strengths [8]. Chromium (Cr) is prized for its inherent hardness and high resistance to all types of corrosion. When chromium is added to nickel alloys, their strength is increased [11].

Samples that are powdered are required for the production process. The following elemental powders are bought from Oxford lab chemicals: Ti (99.5% pure, 325 mesh size), Al (99.5% pure, 325 mesh size), Ni (99.5% pure, 200 mesh size), Cr (99.5% pure, 200 mesh size), Co (99.5% pure, 325 mesh size), and Fe (99.5% pure, 270 mesh size).

4.2 MECHANICAL ALLOYING

One type of nonequilibrium powder solid alloying technique is mechanical alloying. Powder metallurgy is used to create the multi-principal high-entropy alloy's powder, which is then mechanically combined in a ball mill in accordance with the proportions of the alloy's component elements. A block is created by sintering, hot press sintering, or spark plasma sintering the combined powder after it has been put in a mold and compressed. The elemental mixed powder may also be charged into a tube for explosive sintering. The high-entropy bulk sintered alloy may also undergo hot forging, hot rolling, or hot extrusion compaction.

It is advantageous to increase the solid solubility between the primary elements while creating high-entropy alloys mechanically, as this process is more conductive to the creation of high-entropy alloy solid solutions than casting [16-20].

4.2.1 BALL MILLING PROCESS

Ball milling is a grinding method used to effectively combine and crush material into smaller particles. Two or four bowls and one turn disc (turn table) make up the ball mill system. The bowls revolve in the opposite direction from the turn disc, which rotates in the same way. The powder particles undergo high energetic impact during the high-energy ball milling process. The movements of the balls and the powder are depicted in figure 4.1 below.

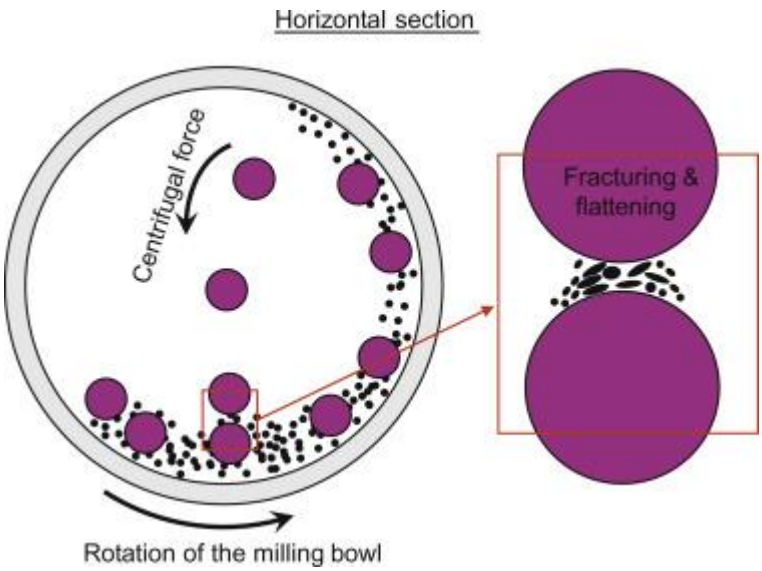

Figure 4.1: Schematic view of motion of the ball and powder mixture.[22].

The Retsch PM 100 high-energy planetary ball mill was used for the alloying process, and the ball-to-powder weight ratio was 10:1.The combined powder is put in a sealed container with

tungsten carbide balls with a diameter of 10 mm, and the ceramic container is rotated at a speed of around 330 revolutions per minute for 360 minutes to ensure that the powder particles are well mixed. To prevent powder from adhering to jars and to minimize powder oxidation, a process control agent must be added throughout the ball milling process. Toluene is used in this instance as a process control agent.

Fig 4.2: Retsch PM 100 high-energy planetary ball mill (IIT Palakkad).

4.2.2 SPARK PLASMA SINTERING PROCESS

The Field Assisted Sintering Technology (FAST), Pulsed Electric Current Sintering (PECS), and Electric Pulse Assisted Consolidation (EPAC) are other names for the Spark Plasma Sintering (SPS) process. Spark plasma sintering (SPS) is employed to create nanocrystalline alloys since the usual sintering technique causes nanocrystalline alloy powder to develop into grains [22].

By utilizing spark plasma sintering, the milled powders (TiAlNiCrCo and TiAlNiCrFe samples) were consolidated into pellets. Spark plasma sintering was done on Dr. Sinter (SPS-625, Fuji -japan) at a temperature of 1000^0C with a heating rate of 100^0C min^{-1} and holding time of 10 min at 1000^0C. (SPS machine specifications :Current : 5000AMax,sintering Temperature : 2000˚ ,Celsius Max. sintering pressure : 100 KN, Vacuum : up to 0.006 Pa). SPS was performed using punches with a 20 mm diameter and a hollow, cylindrical die constructed of high-density graphite that had an inner diameter of 20.5 mm, an exterior diameter of 50 mm,

and a height of 40 mm. For simple sample removal from the die after sintering and to facilitate thermal and electrical conduction, 0.2 mm thick graphite foils were wrapped around the inner diameter.

Fig 4.3: Spark Plasma Sintering (SPS) Machine (IIT Madras).

Thermal energy is employed throughout the sintering process to create goods with a certain density. Solid state sintering, liquid state sintering, viscous flow sintering, and transient liquid phase sintering are the four main divisions of this method. The sintering in the SPS often falls under the categories of solid state, transient, and/or liquid phase sintering. Figure 4.4 displays a schematic illustration of an SPS unit.

In that the powder is put into a pressure die and subjected to a variable uniaxial pressure throughout the sintering process, the SPS unit is comparable to a standard hot press equipment. A pulsed direct current is run through the sample holder of the SPS apparatus, which is constructed of conductive material (typically graphite), and through the sample in appropriate circumstances. As a result, the pressure dies acts as a heating source. Normal sintering takes place in a water-cooled chamber under vacuum.

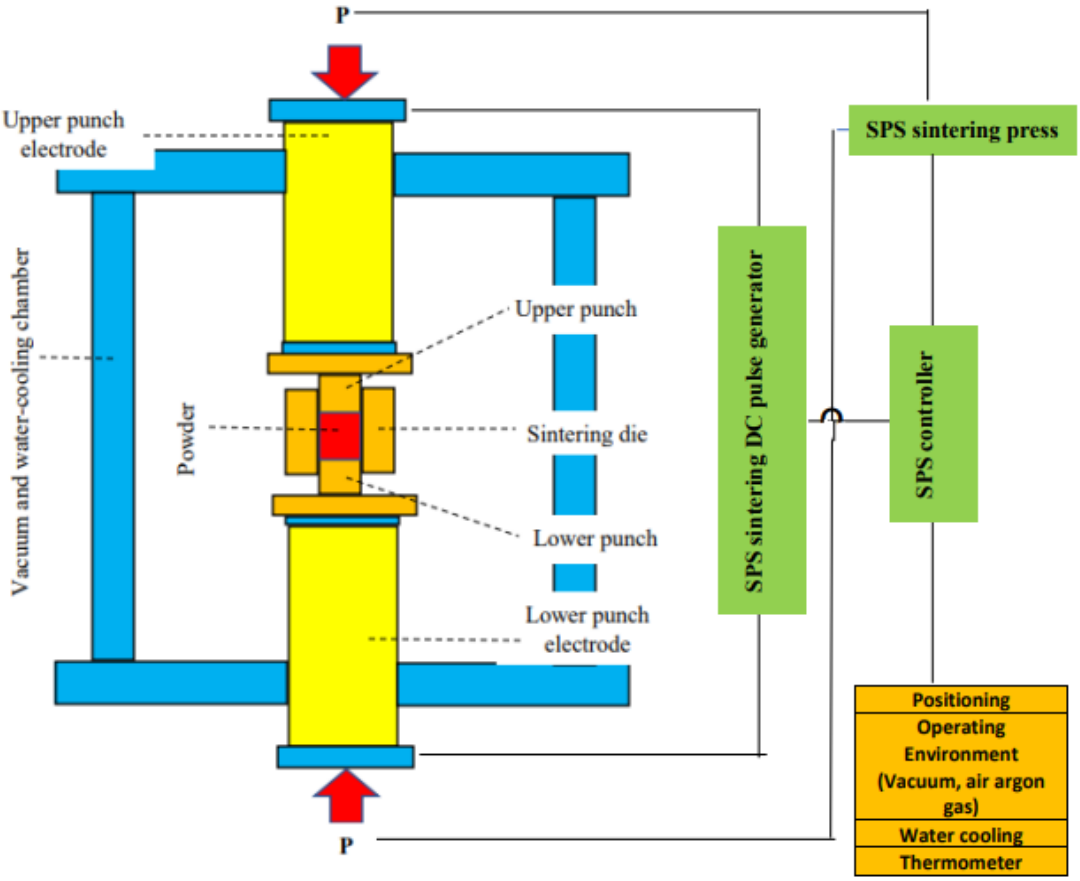

Figure 4.4: Schematic illustration of an SPS.

Following SPS, cylindrical pellets of TiAlNiCrCo and TiAlNiCrFe having 20 mm in diameter and 10 mm in height were produced.

4.3 SAMPLE CUTTING AND POLISHING

It is necessary to have a polished surface for microstructural examination.

4.3.1 EDM WIRE CUTTING

These two cylindrical (TiAlNiCrCo, TiAlNiCrFe) Samples were cut by using EDM (Electrical Discharge Machining) wire cutting (on ULTRACUT F1 EDM machine), and it is a significant manufacturing process with several applications across various industries. EDM wire cutting doesn't entail direct contact between the cutting tool and the workpiece, unlike conventional cutting techniques, therefore there is no tool wear or breakage. Due to its excellent precision and consistency, it is the perfect procedure for producing components. EDM wire cutting provides excellent finishes without burrs or jagged edges. This qualifies it for the production of items like aerospace and medical implant components that need a high-quality finish. Fig 4.5 is the wire cut EDM machine (ULTRACUT F1) and Fig. 4.6 is the samples after wire cut EDM. After EDM wire cut we got 4 samples (2nos of TiAlNiCrCo & TiAlNiCrFe).

Fig.4.5: Wire cut EDM machine.

Fig.4.6: Samples after Wire EDM cut.

4.3.2 SAMPLE POLISHING

Samples were polished to a mirror-like surface in preparation for analysis. Using emery sheets of grades 400, 600, 800, 1000, and 4000, all of the sectioned samples were polished. And for the final polishing, a two-hour buffing process using diamond paste is performed on a double disc polishing machine (fig. 4.7). Fig 4.8(a, b) shows the polished samples of TiAlNiCrCo, TiAlNiCrFe.

Fig.4.7: Double Disc Polishing Machine.

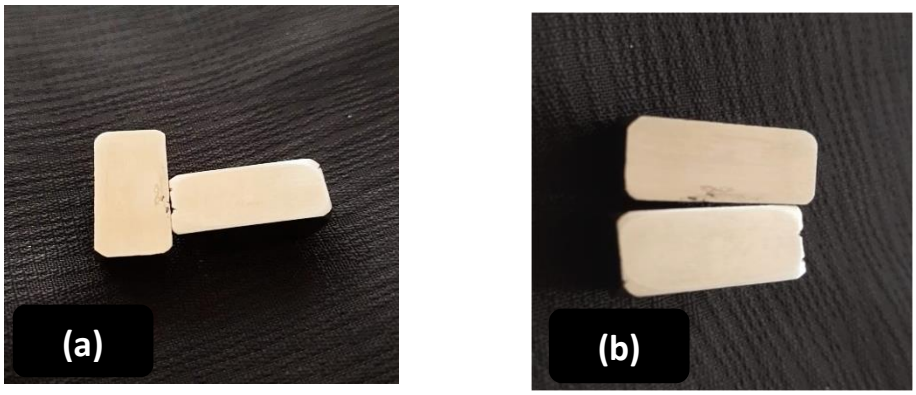

Fig 4.8: Polished samples of (a)TiAlNiCrFe, (b)TiAlNiCrCo.

4.4 CRYOGENIC TREATMENT

Cryogenic treatment is a procedure that includes subjecting materials to extremely low temperatures for a lengthy period of time, usually below -150 °C (-238 °F). The procedure aims to improve the material's mechanical and physical qualities, leading to better performance and durability [19].

Cutting tool production frequently employs cryogenic treatment because it can enhance the tool's functionality and lengthen its lifespan. In order to increase the strength and longevity of the materials used in various components and parts, the procedure is widely employed in other sectors, including automotive, aerospace, and medical.

In general, cryogenic treatment has gained popularity as a method for improving the characteristics of many materials, delivering greater performance and prolonged service life, resulting in cost savings and increased efficiency [2,4,5].

4.4.1 CRYOGENIC TREATMENT USING LIQUID NITROGEN

Liquid nitrogen cryogenic treatment is a common technique for subjecting materials to extremely low temperatures. By chilling and compressing air, liquid nitrogen, an odorless, colorless, and non-toxic liquid, is created. Due to its capacity to quickly cool materials to extremely low temperatures, it is frequently employed in cryogenic applications. Its boiling point is -196°C.

The material is often put in a chamber that has been carefully built and chilled using liquid nitrogen in cryogenic treatment. To allow for the molecular modifications, the substance is kept at the low temperature for a certain amount of time, often several hours. After then, the temperature is gradually increased, and the material is let hours or days to recover to room temperature.

Cutting tools are frequently subjected to cryogenic treatment using liquid nitrogen, which increases the tool's wear resistance and durability. Additionally, it is applied in the automobile sector to increase the efficiency and robustness of engine parts. Additionally, it may be utilized to enhance the characteristics of materials including composites, ceramics, and polymers [2,10]. While applying liquid nitrogen to a material during cryogenic treatment can be a successful way to improve its qualities, it is crucial to remember that in order to prevent thermal shock or other damage to the material, it must be done cautiously and with the right tools [19].

4.4.2 CRYOGENIC TREATMENT SETUP

The completed cryogenic treatment setup is shown in Figure 4.9. Spark plasma sintered TiAlNiCrCo, TiAlNiCrFe alloys were soaked in liquid nitrogen for 4, 8-hour and then allowed to cool to room temperature. Specifically, one sample of TiAlNiCrCo & TiAlNiCrFe was treated for 4-hour, while another sample of TiAlNiCrCo & TiAlNiCrFe was treated for 8-hour.

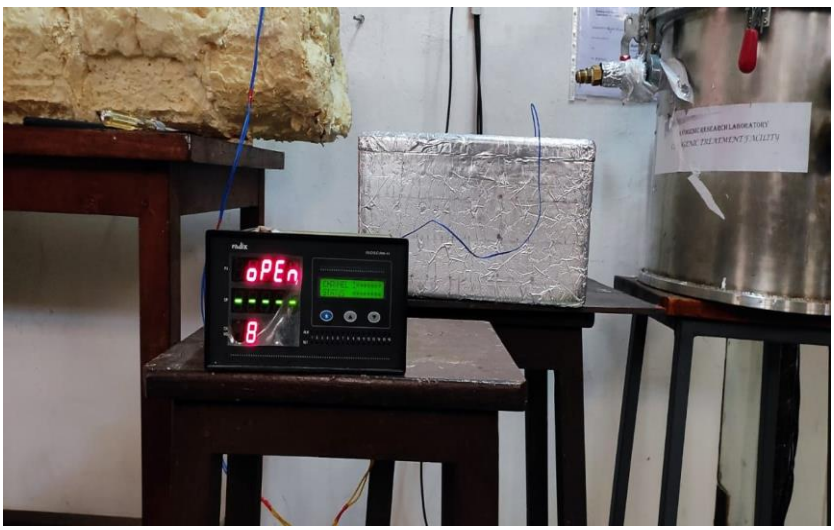

Fig. 4.9: Cryogenic Treatment Setup.

Figure 4.10 gives the schematic diagram of cryogenic treatment setup. A T-type thermocouple that is attached to DAQ is used to measure the temperature. A typical form of thermocouple used to detect temperature in a number of applications is the T-type thermocouple. Two distinct metal wires, commonly copper and constantan, make up the T-type thermocouple. The thermocouple junction, which is formed by joining the two wires at the sensor end, has a temperature range of -200°C to +350°C (-328°F to +662°F).

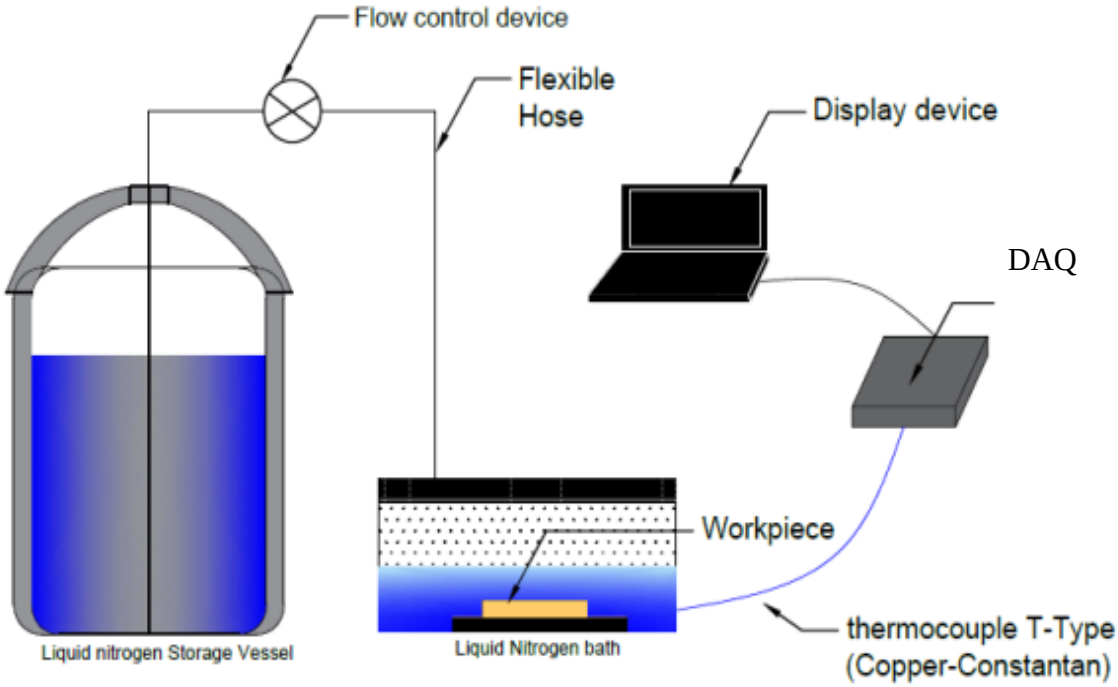

Figure 4.10: Schematic diagram of cryogenic treatment setup.

The great precision of the T-type thermocouple, which is generally within 0.5% of the recorded temperature, is one of its key advantages. It is a popular option for a variety of applications since it is also quite affordable and simple to use. Fig 4.11 is the samples after cryotreatment.

Fig 4.11: Samples after cryotreatment.

4.5 MICROSTRUCTURAL CHARACTERIZATION

The microstructure of samples both before and after cryotreatment was examined using a scanning electron microscope (SEM) and X-ray diffraction (XRD) experiments [9]. The composition of the phases was examined using energy-dispersive spectroscopy (EDS), which also served to verify that the elements had been evenly distributed across the lattice. The analysis was conducted in Central Instrumentation Facility (CIF) at IIT Palakkad.

4.5.1 SEM AND EDX ANALYSIS

In materials science and engineering, advanced technologies like SEM (Scanning Electron Microscopy) and EDX (Energy Dispersive X-ray Spectroscopy) examination are used to learn more about a sample's surface and elemental makeup. An x-ray technique called Energy Dispersive X-Ray Analysis (EDX), often known as EDS or EDAX. A beam of electrons is used in the SEM technique to produce high-resolution pictures of a sample's surface. SEM pictures can provide details on a sample's surface morphology, topography, and texture, enabling the close analysis of microstructural details. By combining SEM with EDX analysis, it is also possible to examine the surface chemistry of a material. Using SEM and EDX analysis together reveals important details about a sample's surface shape and elemental makeup. While EDX can offer details on the elemental composition of certain regions of interest within a sample, SEM pictures can show the surface features and microstructural characteristics of a sample. These approaches may be used in combination to examine the microstructural

characteristics and elemental composition of a variety of materials, such as metals, ceramics, polymers, and composites.

Fig. 4.12.SEM and EDX Analysis equipment [IIT Palakkad].

Geminisem300 (Carl Zeiss) Scanning Electron Microscope with Energy Dispersive Spectroscopy (EDS or EDX) was used to analyze the microstructure of the alloys. Above figure 4.12 is the Scanning electron microscope setup. Thus, before and after cryotreatment, alloys are subjected to SEM and EDX analyses, and microstructure changes are noticed. Spot analysis chemical composition is also noted and investigated.

4.5.2 XRD ANALYSIS

X-ray diffraction (XRD) analysis is an effective non-destructive method for determining the crystalline phases contained in a material and consequently revealing information about its chemical composition. Phase identification is accomplished by contrasting the obtained data with that found in reference databases. Materials are made up of tiny crystal-like structures. ‘Phase' refers to these crystals' chemical composition and structural kind. Materials can include crystalline and non-crystalline components and can be single phases or multiphase combinations. Different crystalline phases produce various diffraction patterns in an X-ray diffractometer. By comparing X-ray diffraction patterns from unknown materials to patterns from reference databases, phase identification may be carried out.

XRD Smart Lab (Rigaku) X- ray diffractometer (fig. 4.13) was used to do analysis with a copper anode Kα radiation, step size of 0.02^0 from 0° to 90°. XRD patterns were recorded at room temperature conditions.

Fig. 4.13: XRD analysis equipment [IIT Palakkad].

4.6 HARDNESS TEST

Hardness tests were done with Vickers microhardness tester (MATRIX P1Vickers-Fig.4.14) at a load of 1000 gf with a 10s loading time. To get the findings, ten tests were run on each sample. A Vickers indenter applied to a surface with a specified force, is used in the Vickers hardness test. Hardness measurements were made by measuring the diagonals of the indentation. Once the indentation is complete, the resultant indent is optically examined to measure the diagonal lengths and ascertain the size of the impression.

Fig. 4.14. Micro Vickers Hardness Testing Machine [CET Trivandrum].

CHAPTER 5

RESULTS AND DISCUSSION

5.1 MICROSTRUCTURE ANALYSIS BEFORE CRYOGENIC TREATMENT

5.1.1 EVOLUTION OF CRYSTAL STRUCTURE THROUGH XRD

The XRD examination of TiAlNiCrFe and TiAlNiCrCo following SPS, that is, prior to cryotreatment, is shown in figures 5.1 and figure 5.2. All of these alloys form two-phase BCC structures following SPS, as seen by the XRD patterns. phase BCC1 (B2 phase) and phase BCC2. BCC1(B2 phase) peaks correspond to those of Ni-Al while BCC2 phase has been identified as a Cr/Cr-Fe, type BCC.

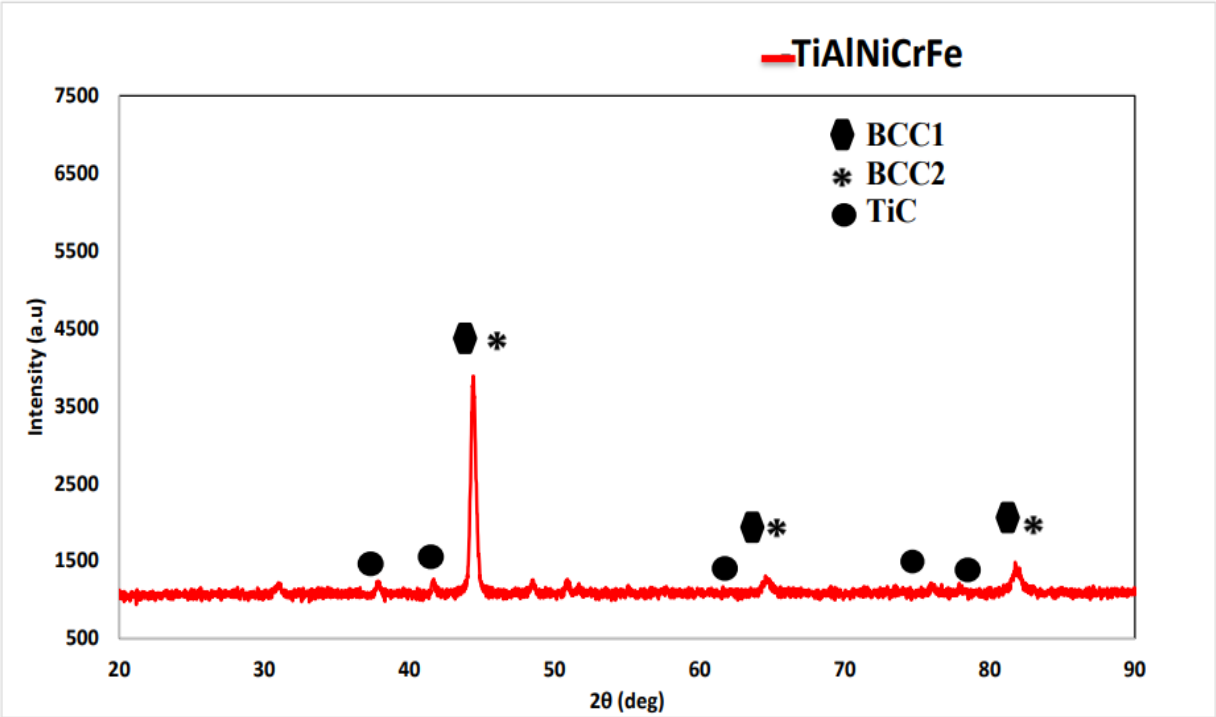

Fig. 5.1: XRD patterns of TiAlNiCrFe before cryotreatment.

The predominant BCC phase seems to be rich in Fe and Cr for alloys comprising Cr and Fe (TiAlNiCrFe). Fe diffuses into Cr due to the higher melting point of Cr (1857 ^{0}C) than that of Fe (1538 ^{0}C), making the unit cell richer in Cr and Fe [20].

Figure 5.2 below shows XRD analysis of TiAlNiCrCo. It forms two BCC phases, much like TiAlNiCrFe alloy. Ni-Al is represented by the BCC1 (B2) peaks, while Cr is the only element in the BCC2 phase. TiAlNiCrCo also exhibits very small FCC phase due of the presence of Co.

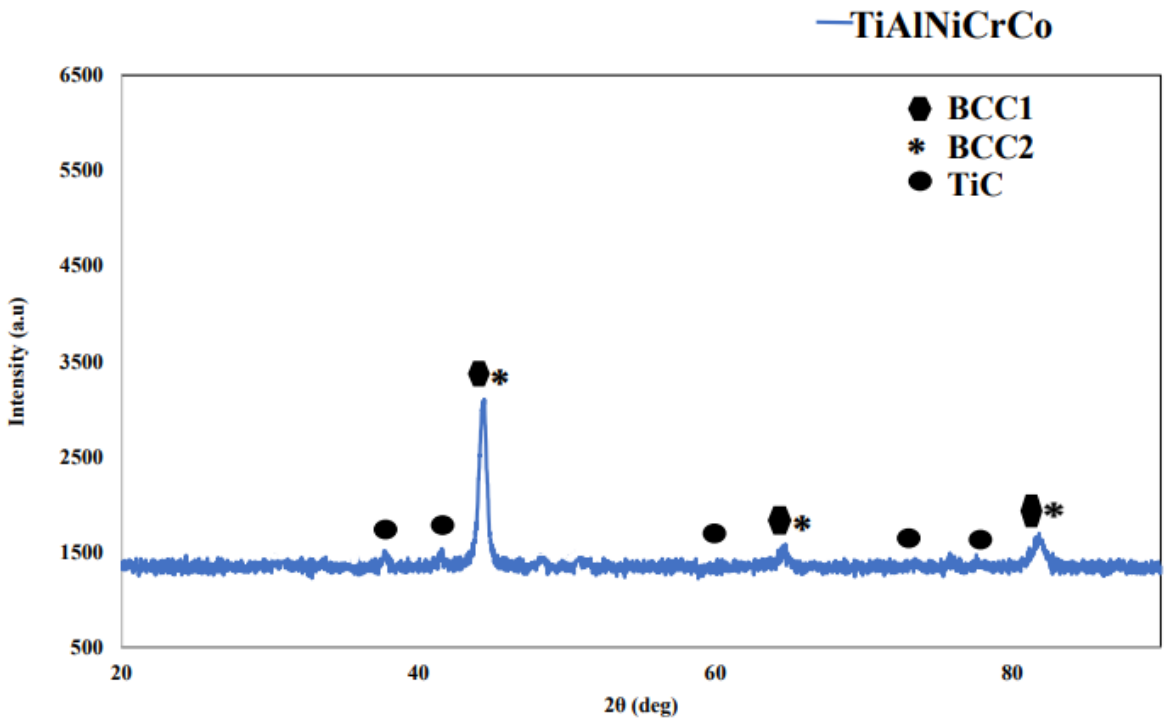

Fig. 5.2: XRD patterns of TiAlNiCrCo before cryotreatment.

In both alloys, there are also tiny peaks suggesting TiC, which shows that the alloy also has carbide dispersion that results from high-temperature sintering. Due to toluene's breakdown during toluene-based Ti milling, considerable carbon contamination may occur [23-26].

5.1.2 MICROSTRUCTURAL CHARACTERIZATION

The SEM back scattered images of the TiAlNiCrFe alloy cross section following SPS are shown in Figure 5.3(a-c).

- TiAlNiCrFe alloy after SPS.

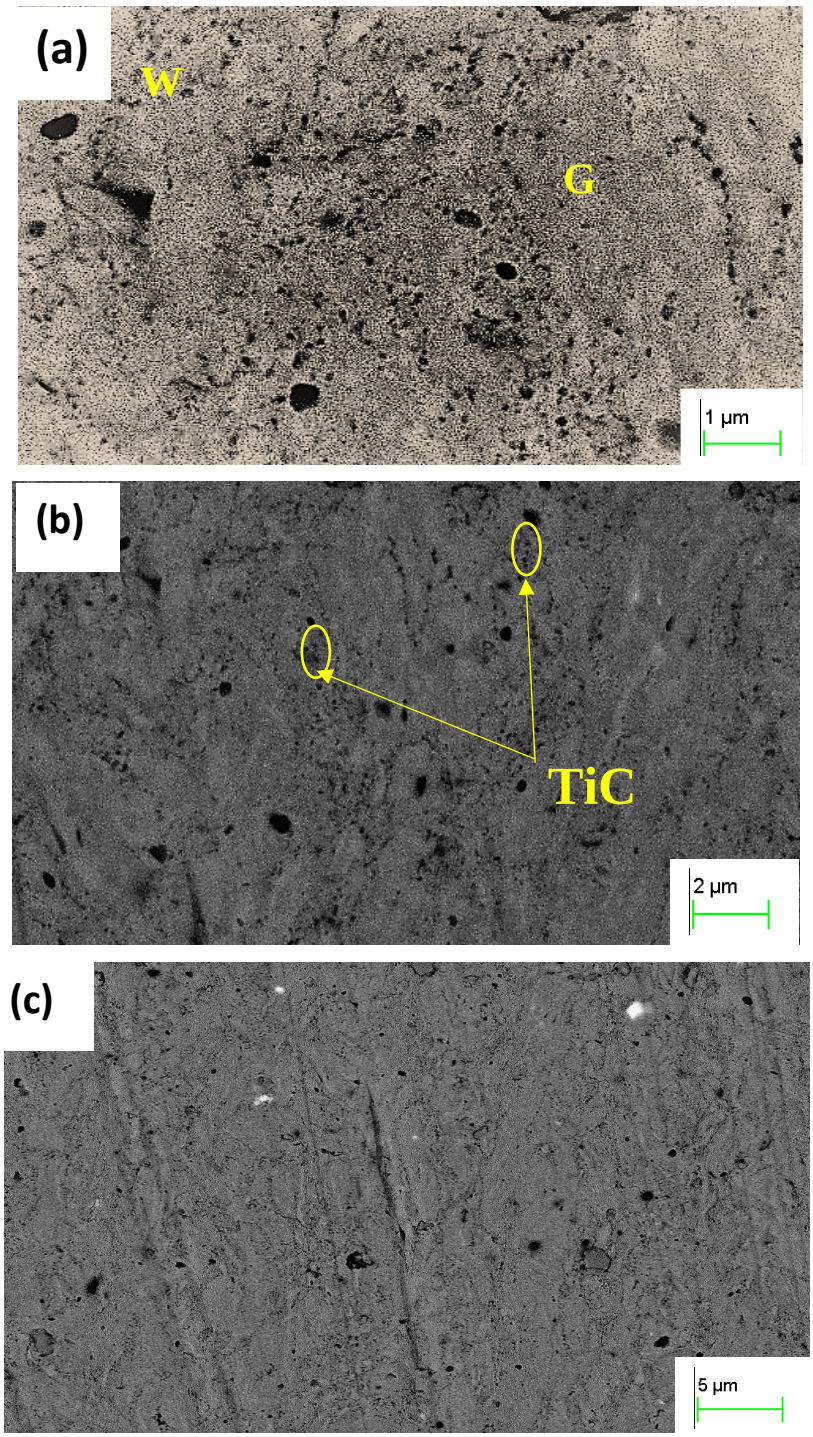

Fig 5.3: (a -c) Back scattered images of the polished cross section samples after SPS of TiAlNiCrFe.

In these BSE pictures, two-phase zones may be detected, which is denoted by the letters "W" and "G" stand for white and grey, respectively, on a map. TiC, which is an SPS-derived contaminant, is shown by black dots particles scattered throughout the matrix [20,23]. Figure 5.4 (a-e) displays the elemental mapping of the whole TiAlNiCrFe alloy.

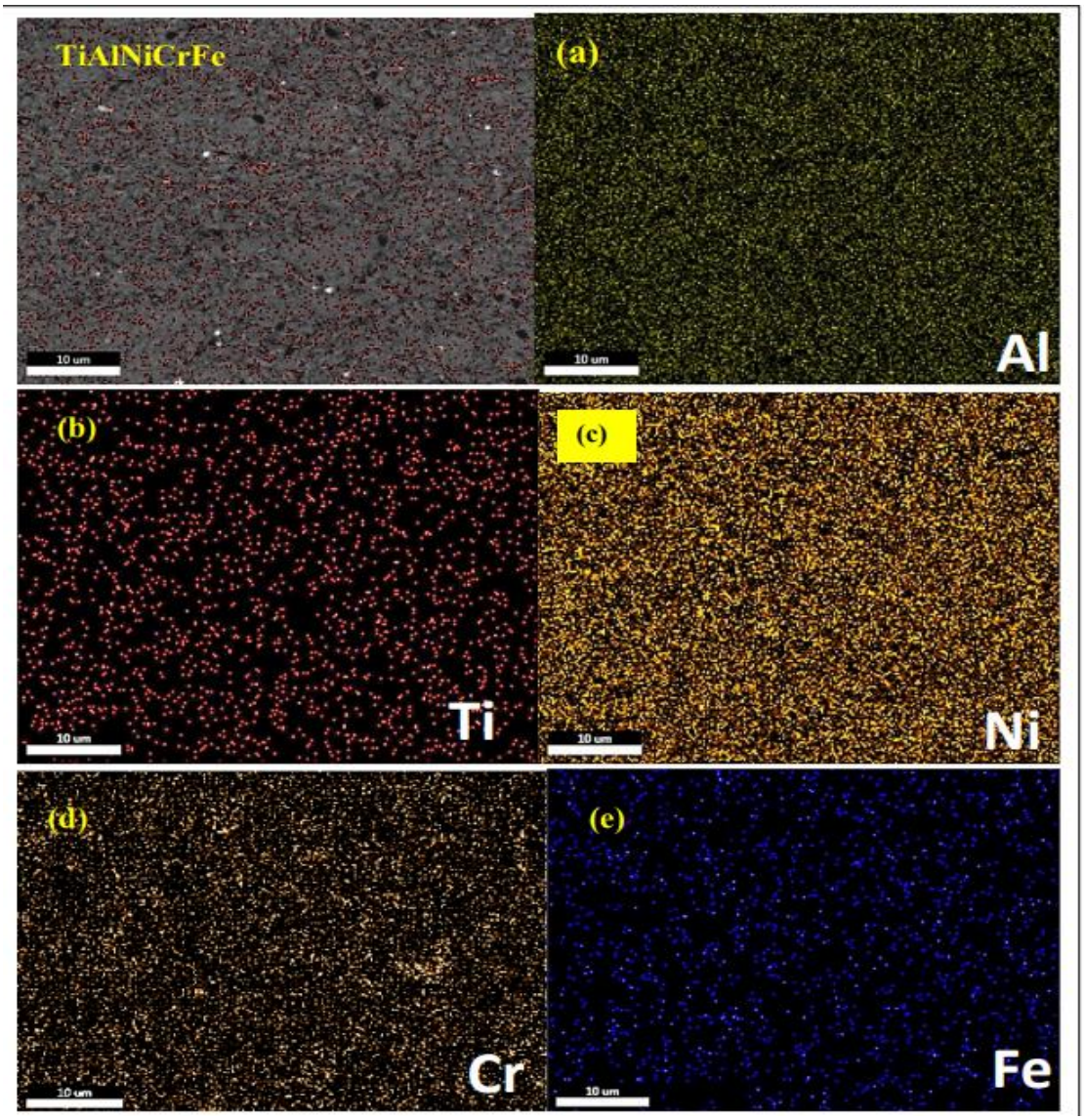

Fig 5.4: (a-e) EDS elemental mapping of TiAlNiCrFe.

The elemental composition of the material in the analyzed spot may be determined using the information gleaned from the TiAlNiCrFe alloy's EDS spot analysis. In particular, the energy of the X-rays picked up by the EDS detector matches the energy of the distinctive X-rays given off by the elements in the sample. It is possible to ascertain the elemental composition of the sample at the analyzed spot by examining the energy and intensity of these X-rays.

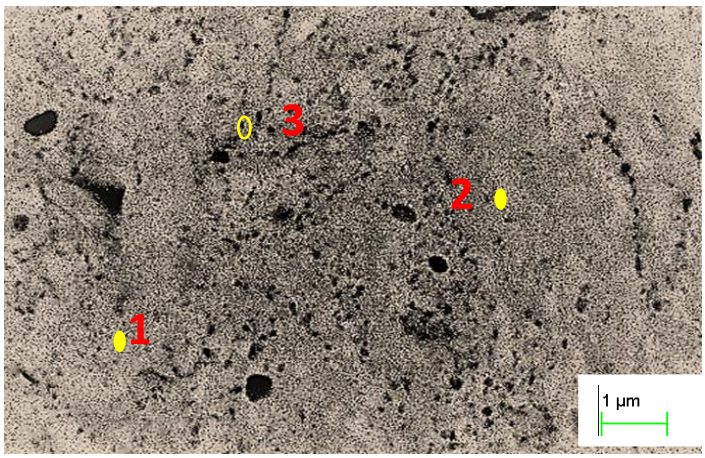

Fig 5.5: EDS Spot Analysis of TiAlNiCrFe specimen after SPS.

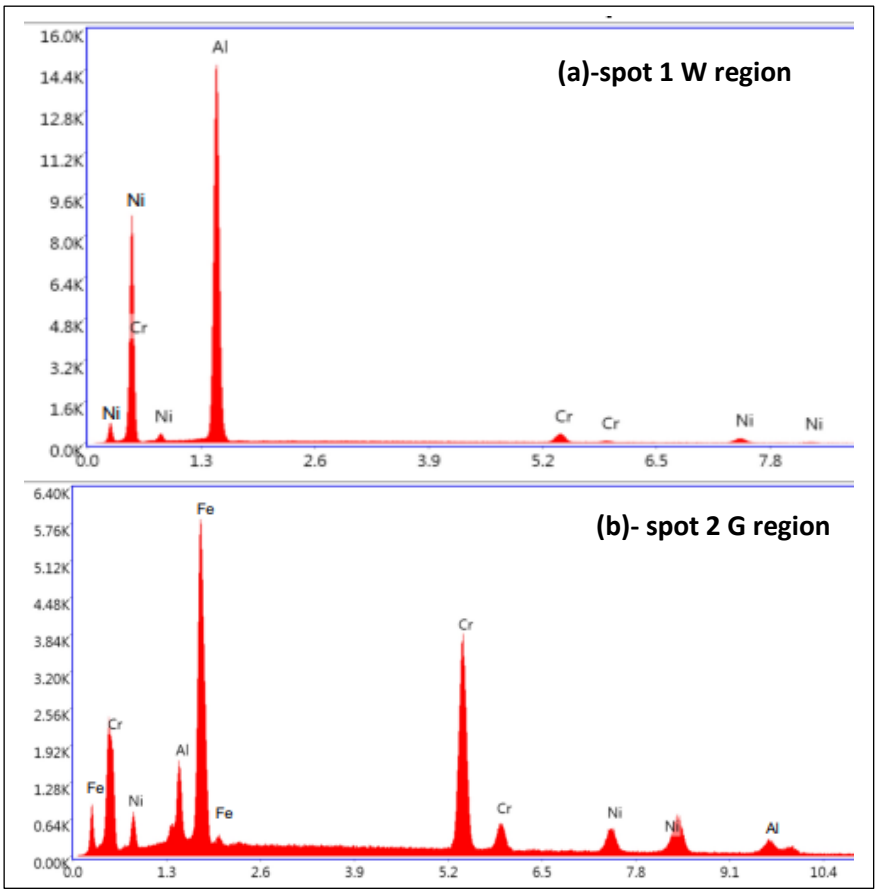

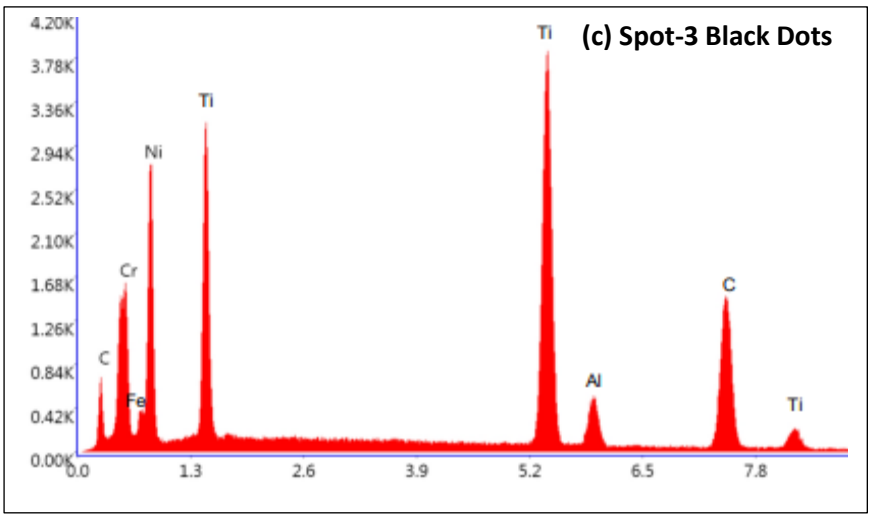

Fig 5.6.(a-c): Graph of EDS spot Analysis of TiAlNiCrFe alloy after SPS.

The TiAlNiCrFe alloy was subjected to an EDS spot analysis following SPS, as shown in EDS spot graph figure 5.6 (a-c). From the spot analysis the average elemental composition on the spotted regions are evaluated and displayed in table 5.1.

It is clear from the graph that BCC1 (B2) (the white phase-spot 1) is rich in Ni-Al type, whereas BCC2 (the grey phase -spot 2) is of Cr-Fe type. TiC, which is an SPS-derived contaminant [23], is shown by black dots particles scattered throughout the matrix(spot3).

Table 5.1 Average Composition of elements on different spots (TiAlNiCrFe).

Elements	**Spot 1-W region (at%)**	**Spot 2-G region (at%)**	**Spot-3 (at%)**
Ti	-	-	39.02
Al	53.2	11.70	9.14
Ni	38.35	13.03	14.75
Cr	8.45	39.35	12.33
Fe	-	35.92	6.41
C	-	-	18.35

The TiAlNiCrFe alloy was subjected to an EDS area analysis following SPS, as shown in above figure 5.4. Each elemental mapping (figure 5.a-e) reveals the alloy's particular chemical composition, and table 5.2 shows its elemental composition.

Table 5.2: Composition of elements TiAlNiCrFe after SPS.

ELEMENT	Composition of elements (at%)
Ti	9.45
Al	27.8
Ni	30.47
Cr	23.55
Fe	8.73

- TiAlNiCrCo alloy after SPS.

The SEM back scattered images of the TiAlNiCrCo alloy cross section following SPS are shown in Figure 5.7(a -c). The white (W) and gray (G) region is more visible is this alloy. Similar to TiAlNiCrFe alloy, it forms two BCC phases. The BCC1(B2) peaks correspond to Ni-Al, while the BCC2 phase contains solely Cr. Due to Co, TiAlNiCrCo also displays a very small negligible FCC phase.

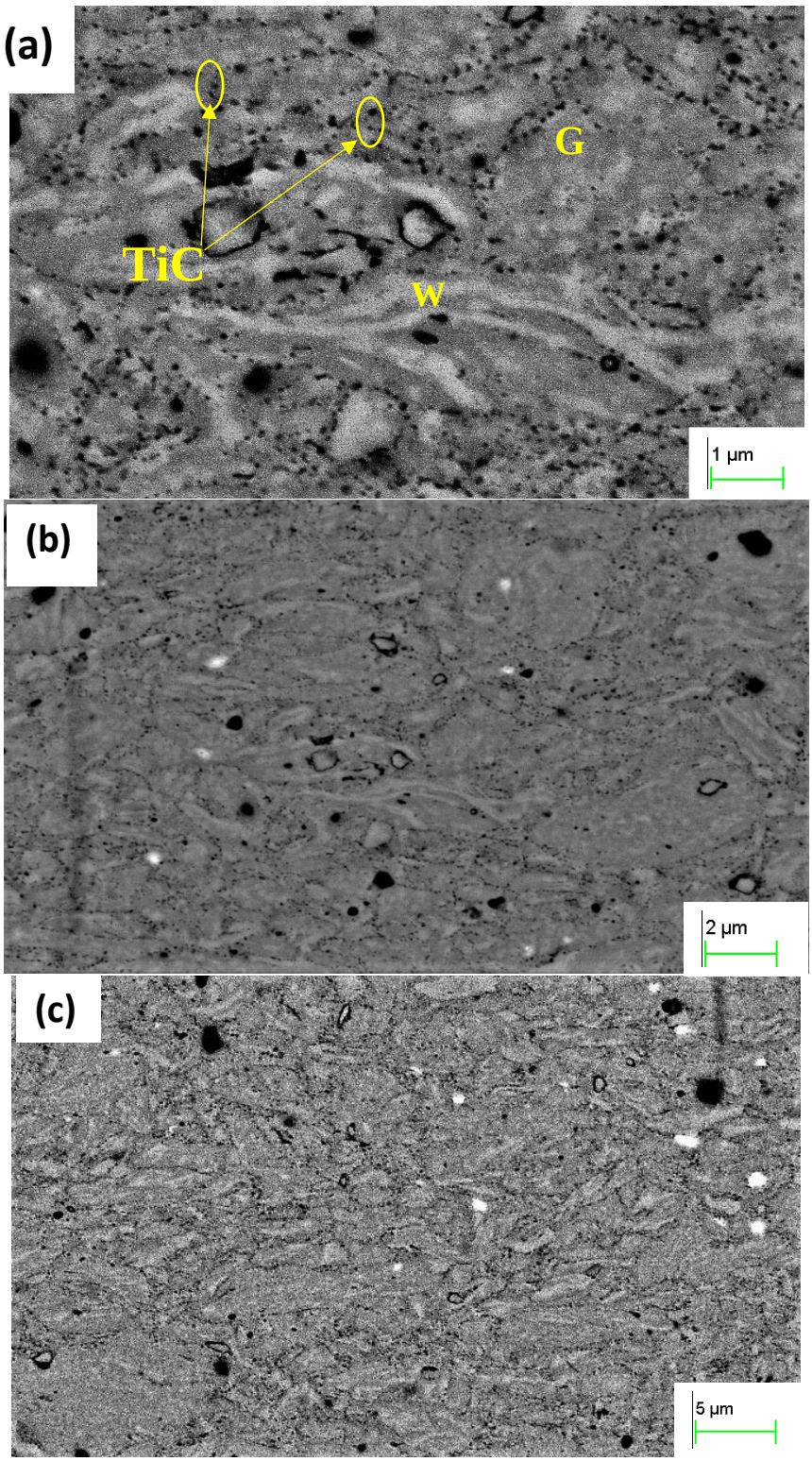

Fig 5.7.(a-c): Back scattered images of the polished cross section samples after SPS of TiAlNiCrCo.

TiC, a contaminant from SPS, is indicated by black dots particles scattered throughout the matrix. The data from the TiAlNiCrCo alloy's EDS spot analysis may be used to identify the elemental composition of the material. Figure 5.8 (a-e) displays the elemental mapping of the whole TiAlNiCrCo alloy.

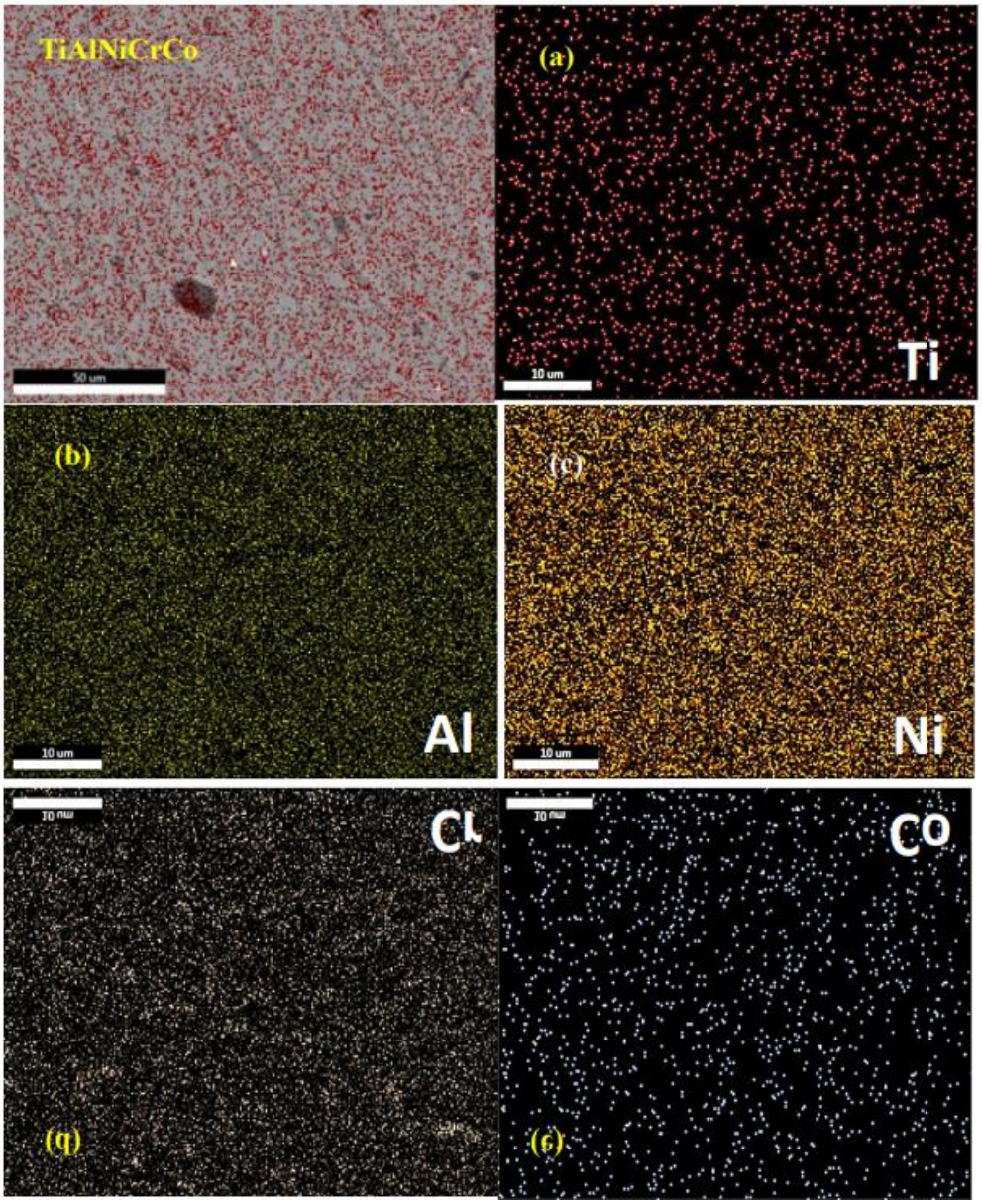

Fig 5.8: (a-e) EDS elemental mapping of TiAlNiCrCo.

From the EDS elemental area mapping we can find out the composition of elements distributed the samples. Table 5.3 gives the at% of composition of elements.

Table 5.3: Composition of elements TiAlNiCrCo after SPS

ELEMENT	Composition of elements (at%)
Ti	10.85
Al	26.20
Ni	24.34
Cr	29.10
Co	9.51

The TiAlNiCrCo alloy was subjected to an EDS spot analysis to find the elemental composition on different regions like white, gray regions, following SPS, as shows below figure 5.9. The information obtained from the EDS spot analysis of the TiAlNiCrCo alloy may be used to identify the elemental composition of the material in the analyzed spot. The energy of the X-rays detected by the EDS detector specifically matches the energy of the unique X-rays emitted by the components in the sample [29,30]. By looking at the energy and intensity of these X-rays, it is feasible to determine the elemental composition of the material at the analyzed location. Each spot graph (figure 5.10a-c) reveals the alloy's particular chemical composition, and table 5.4 shows its elemental composition.

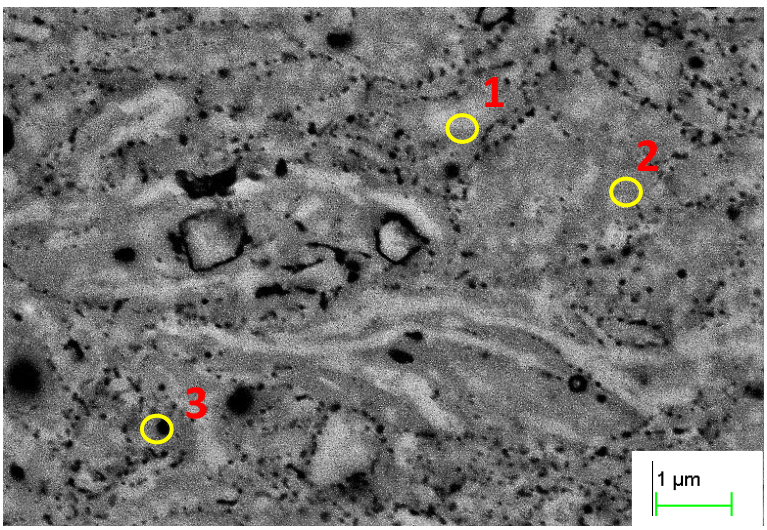

Fig 5.9: EDS Spot Analysis of TiAlNiCrCo specimen after SPS.

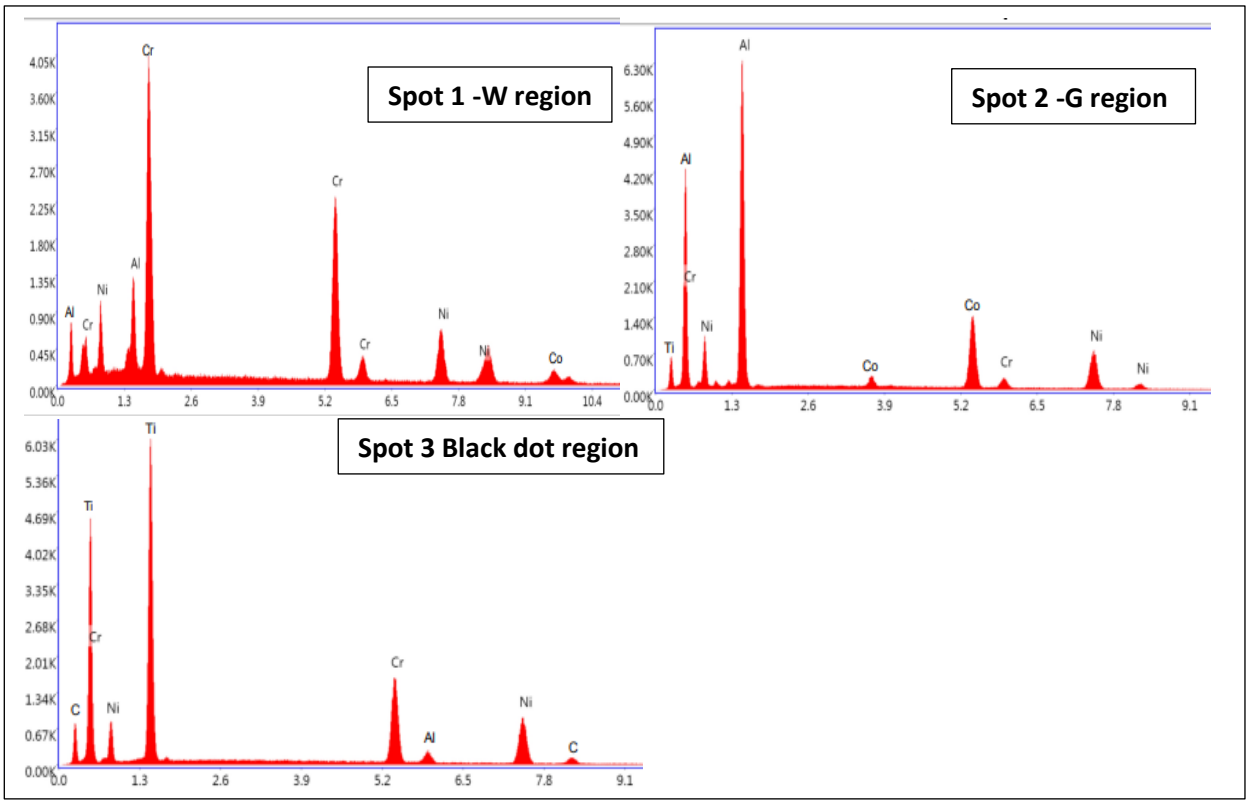

Fig 5.10.(a-c): Graph of EDS spot Analysis of TiAlNiCrCo alloy after SPS.

Table 5.4 Average Composition of elements on different spots.

Elements	**Spot 1-W region (at%)**	**Spot 2-G region (at%)**	**Spot-3 (at%)**
Ti	1.08	-	37.13
Al	48.3	12.34	14.5
Ni	33.4	14.86	16.73
Cr	11.2	66.57	17.31
Co	6.02	6.23	-
C	-	-	14.33

.

The graph clearly shows that BCC1 (B2-white phase), which is rich in Ni-Al type, differs from BCC2 (the grey phase), which contains just Cr.

5.1.3 MECHANICAL PROPERTIES

Vickers microhardness tests were conducted with a load of 1000 gf and a loading duration of 10s. To get the findings, ten tests were run on each sample. The hardness values of TiAlNiCrFe and TiAlNiCrCo are shown in table 5.5.

Table 5.5: Hardness values of samples before cryotreatment.

SAMPLE	HARDNESS VALUE (HV)
TiAlNiCrFe	755 ± 8 HV
TiAlNiCrCo	702 ± 6 HV

From the above table, we can see that the TiAlNiCrFe sample has more hardness than TiAlNiCrCo sample. The presence of cobalt content and large crystallite sizes(fig 5.14) may decrease the hardness of TiAlNiCrCo alloy [20,25-28].

5.2 MICROSTRUCTURE ANALYSIS AFTER CRYOGENIC TREATMENT

Spark plasma sintered TiAlNiCrCo and TiAlNiCrFe alloys were soaked in liquid nitrogen for 4,8-hour after they were allowed to warm to room temperature. DCT is an effective method, which improves the properties of alloys [31-35]. In more detail, one sample of TiAlNiCrCo & TiAlNiCrFe was subjected to a 4-hour treatment, while another sample of TiAlNiCrCo & TiAlNiCrFe was subjected to an 8-hour treatment.

5.2.1 EVOLUTION OF CRYSTAL STRUCTURE THROUGH XRD

TiAlNiCrFe XRD pattern after two distinct deep cryogenic treatment durations (four and eight hours) is shown in Figure 5.11. From the XRD pattern, we can see the two BCC phases. After deep cryogenic treatment, 4hr treated alloys diffraction peak intensity of the BCC phase did not significantly changed as compared to alloy before cryotreatment (fig.5.1).

Sharp peaks or high intensities are a sign of increased arrangement, crystallization, and order. More stronger peaks would result with the same ordering and other experimental settings held

constant. It can be noticed that following deep cryogenic treatment, the diffraction peak intensity of the alloy's crystal surface treated for 8-hour is reduced by comparing the XRD patterns of the sample treated for 4 hrs., that is 4hr treated alloy is more orderly arranged.

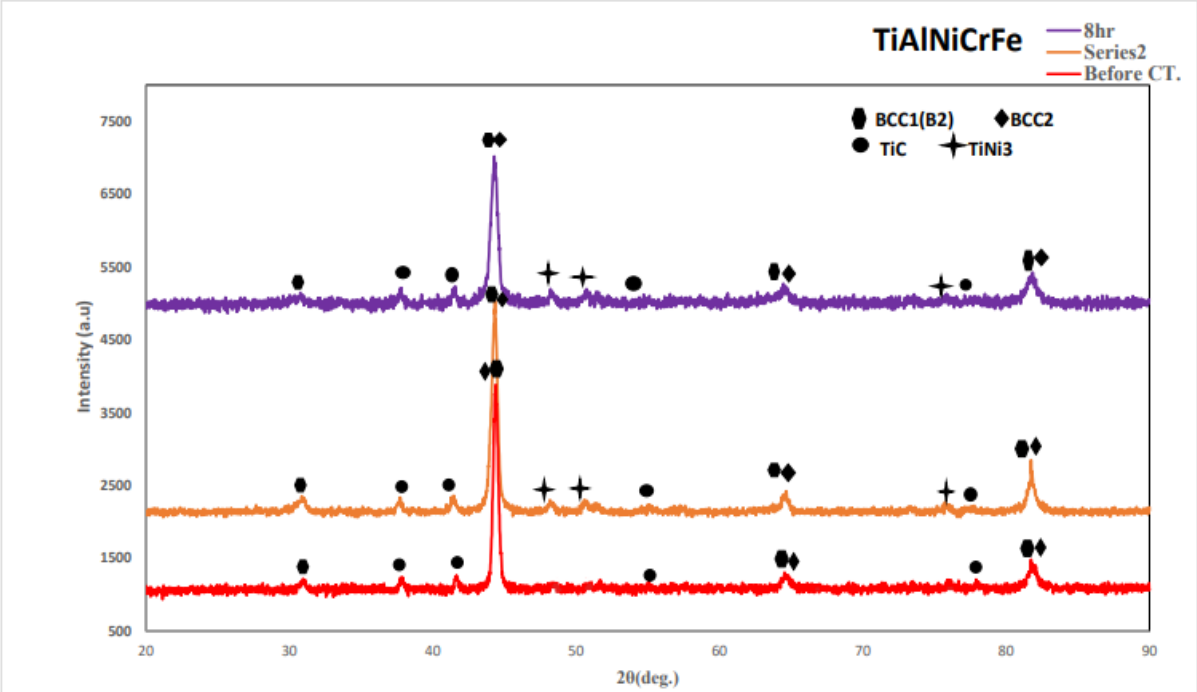

Fig.5.11: XRD patterns of 4hr,8hr cryotreated TiAlNiCrFe alloy.

The findings demonstrate that a 4 hour deep cryogenic treatment did not alter the crystal structure of the alloy compared to non-treated alloy (fig.5.1), but that as the time of the deep cryogenic treatment increased, the diffraction peak intensities gradually reduced in 8hr treated alloy.

The alloy exhibits a prominent BCC line following a 4-hour cryogenic treatment. BCC1 (B2) with NiAl and CrFe-rich BCC2.TiNi3 small peaks are present in both 4hr, 8hr treated alloy, and NiAl type BCC1 (B2) and CrFe rich BCC2 are formed.

Figure 5.12 gives the XRD analysis of 4-hour and 8-hour cryotreated TiAlNiCrCo alloys. From this analysis pattern it shows that 4-hour treated alloys shows large peak intensity than 8-hour treated alloy, similar to 4-hour treated TiAlNiCrFe alloy. Compared to as-sintered alloys pattern both 4-hour and 8-hour treated alloy also shows two main BCC phases NiAl rich BCC1 and Cr only BCC2.

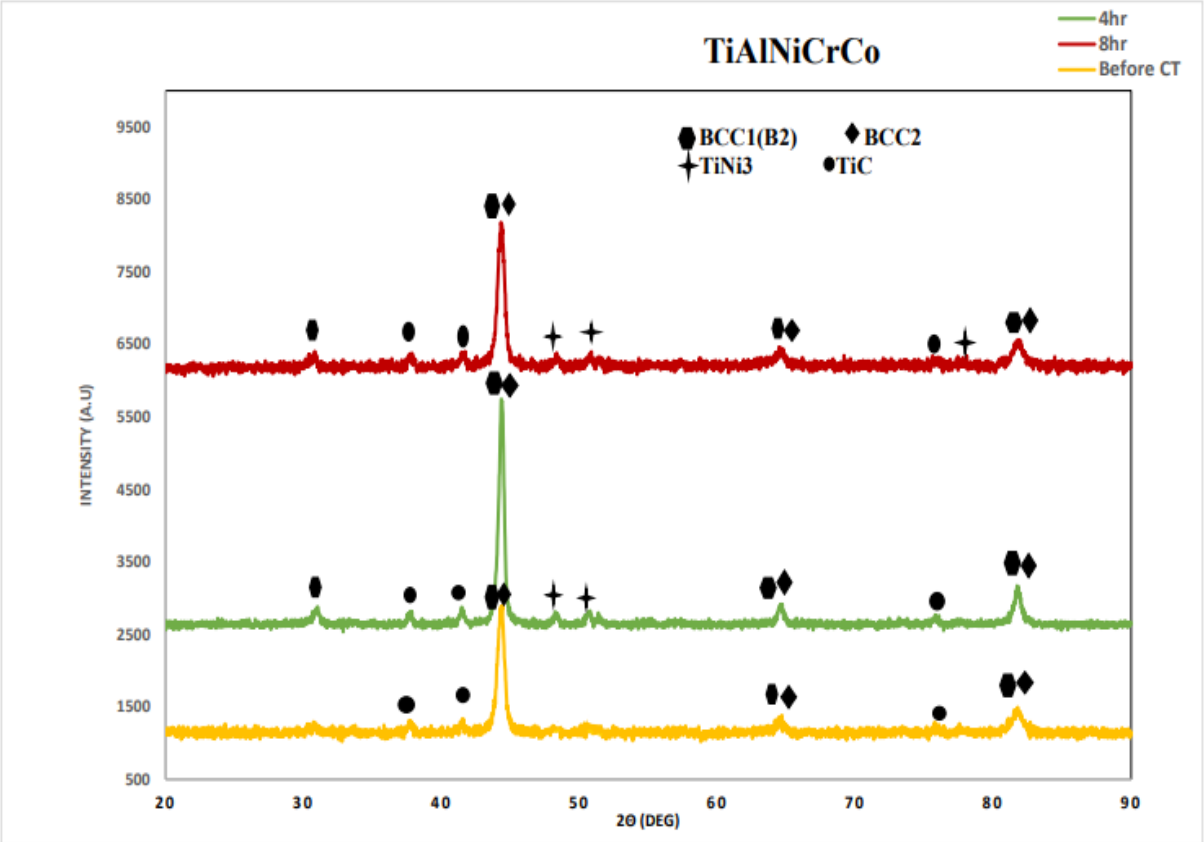

Fig. 5.12: XRD patterns of 4hr,8hr cryotreated TiAlNiCrCo alloy.

From the figure 5.2 (before cryotreatment) TiAlNiCrCo alloy, XRD graph, both 4hr, 8hr treated alloys show small TiNi3 peaks on cryotreatment. All cryotreated alloys (TiAlNiCrFe & TiAlNiCrCo) exhibit small peaks that resemble the as-sintered alloy patterns and indicate TiC.

The crystallite size and lattice strain for the phases in TiAlNiCrFe, TiAlNiCrCo samples before and after cryotreatment is calculated through Williamson-Hall plot method.

The Williamson-Hall plot method is used to determine the crystallite size and lattice strain for the phases in samples. Williamson and Hall proposed employing peak width 2θ as a function to determine size and strain broadening. The broadening (β_T) is due to combine effect of crystallites size (β_D) and micro strain (β_ε).

$$\beta_T = \beta_D + \beta_\varepsilon$$

From the Scherrer equation $D=K\lambda / \beta_D \cos\theta$, we get $\beta_D = K\lambda / D \cos\theta$, where K (shape factor) = 0.9 and λ (wave length) = 0.15406 nm, D is the crystallite size and θ (peak position).

$\beta_\varepsilon = 4\varepsilon \tan\theta$, ($\beta_\varepsilon$-broadening due to strain, ε- is the strain).

$$\beta_T = \beta_D + \beta_\varepsilon$$

$$\beta_T = (K\lambda / D \cos\theta) + 4\varepsilon \tan\theta$$

$$\beta_T \cos\theta = \varepsilon (4 \sin\theta) + (K\lambda / D).$$

Comparing to the standard equation for a straight-line, y = mx+c, (m= slope, c=intercept). Now we see that by plotting ($\beta_T \cos\theta$) versus ($\sin\theta$), we get slope (ε) and intercept ($K\lambda / D$). This plot is known as Williamson-Hall plot. Fig (5.13) is the W-H plot of TiAlNiCrFe before and after (4,8 hr.) treatment and its crystallite size are listed in table (5.6).

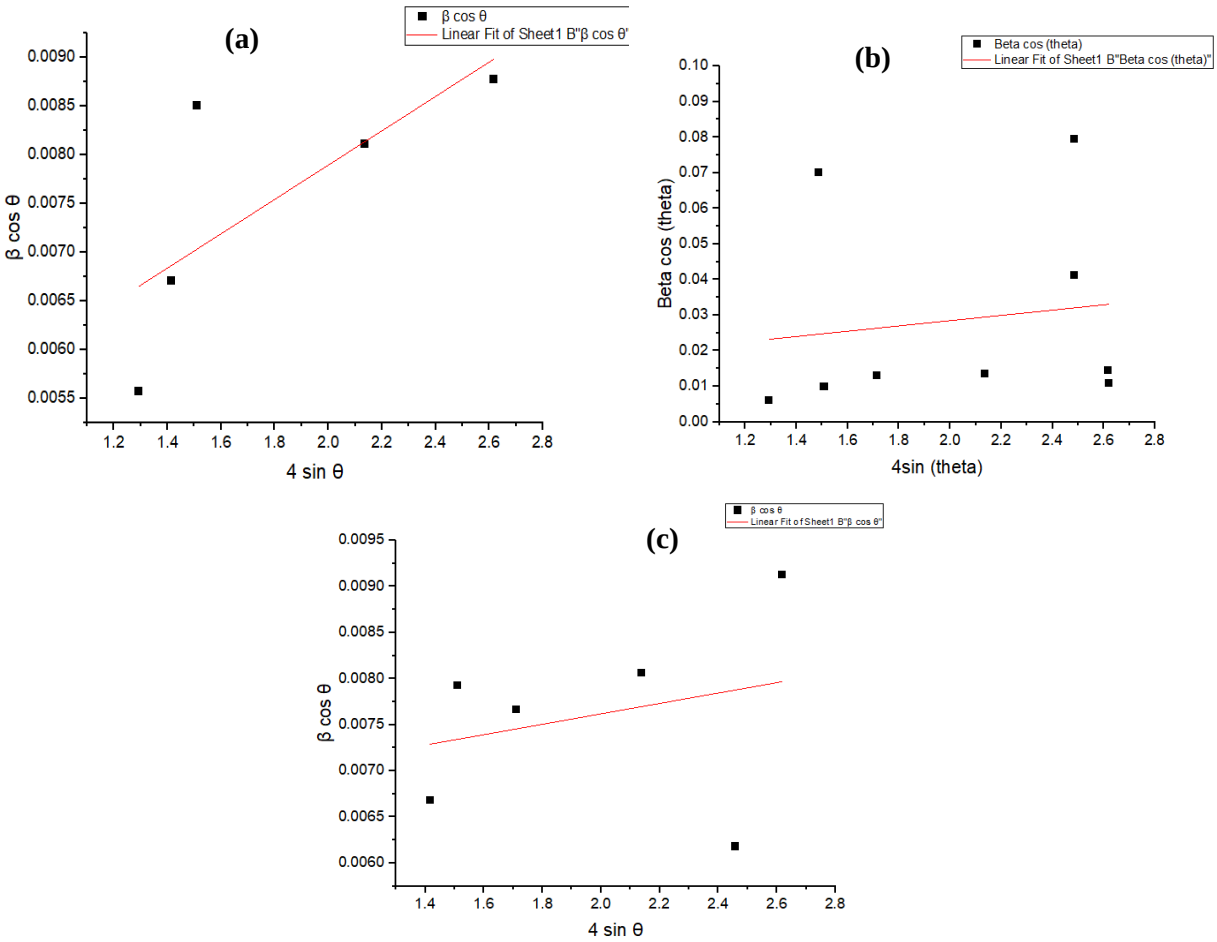

Fig (5.13) is the W-H plot of TiAlNiCrFe before(a) and after CT (b:4hr, c:8hr).

Table (5.6): Crystallite (D) size and Lattice strain of TiAlNiCrFe alloy before and after CT.

Sample	D(nm)	Lattice strain ($\varepsilon*10^{-3}$)
TiAlNiCrFe	22.3	5.6
TiAlNiCrFe (4hr.)	10.6	2.6
TiAlNiCrFe (8hr.)	16.32	3.6

Fig (5.14) is the W-H plot of TiAlNiCrCo before and after (4,8 hr.) treatment and its crystallite size are listed in table (5.7).

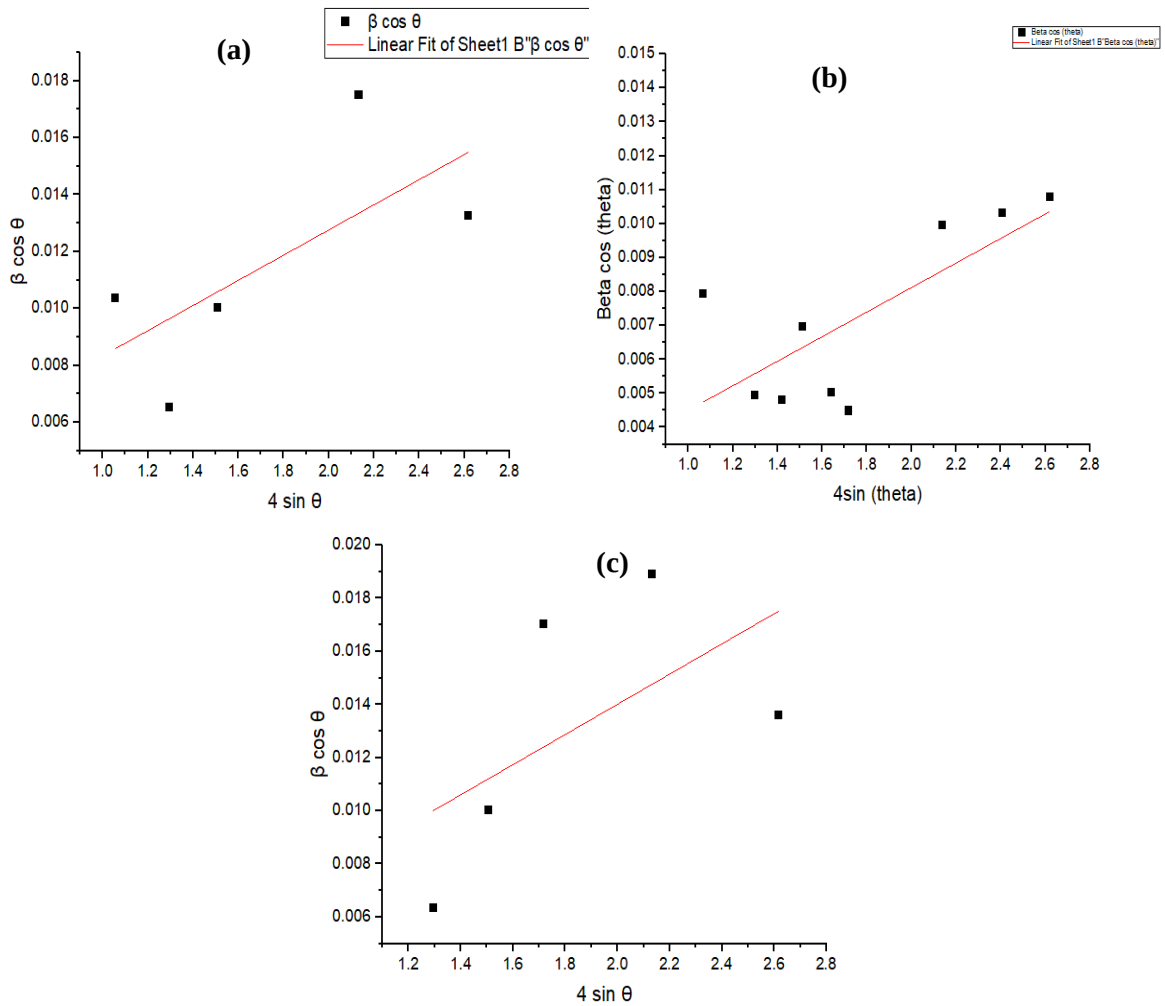

Fig (5.14) is the W-H plot of TiAlNiCrCo before (a) and after CT (b:4hr, c:8hr).

Table (5.7): Crystallite (D) size and Lattice strain of TiAlNiCrCo alloy before and after CT.

Sample	D(nm)	Lattice strain ($\varepsilon*10^{-3}$)
TiAlNiCrCo	**54.6**	**5.6**
TiAlNiCrCo (4hr.)	**33.1**	**1.76**
TiAlNiCrCo (8hr.)	**37.0**	**4.4**

From the table (5.6, 5.7) it is evident that the crystallite size is decreased in both cryotreated samples (TiAlNiCrFe, TiAlNiCrCo) as compared to nontreated samples. Crystallite size first decreased in 4hour and increased for 8hour treatment. Thus, we can understand that the cryotreatment process reduce the crystallite size of both HEAs alloys [38-42].

5.2.2 MICROSTRUCTURAL CHARACTERIZATION

- 4hours treated TiAlNiCrFe sample 1.

The SEM back scattered images of the 4hr treated TiAlNiCrFe alloy cross section following SPS are shown in Figure 5.15(a -c).

The letters "W" and "G" stand for white and grey, respectively, on a map, and they indicate two-phase zones, which can be seen in these BSE images. BCC1and BCC2, and the phases are well arranged and more visible in BSE images. The elements are uniformly distributed all over the alloy. The kind and distribution of components in the BCC phases before and after deep cryogenic treatment did not significantly alter, as can be observed in figure 5.15. BCC1(B2) shows Ni-Al rich face and BCC2 shows Cr-Fe phase The two BCC phases that were generated in the TiAlNiCrFe alloy appear to be of such fine size that high resolution may be required to discriminate between them, according to the uniform dispersion of the elements in the alloy.

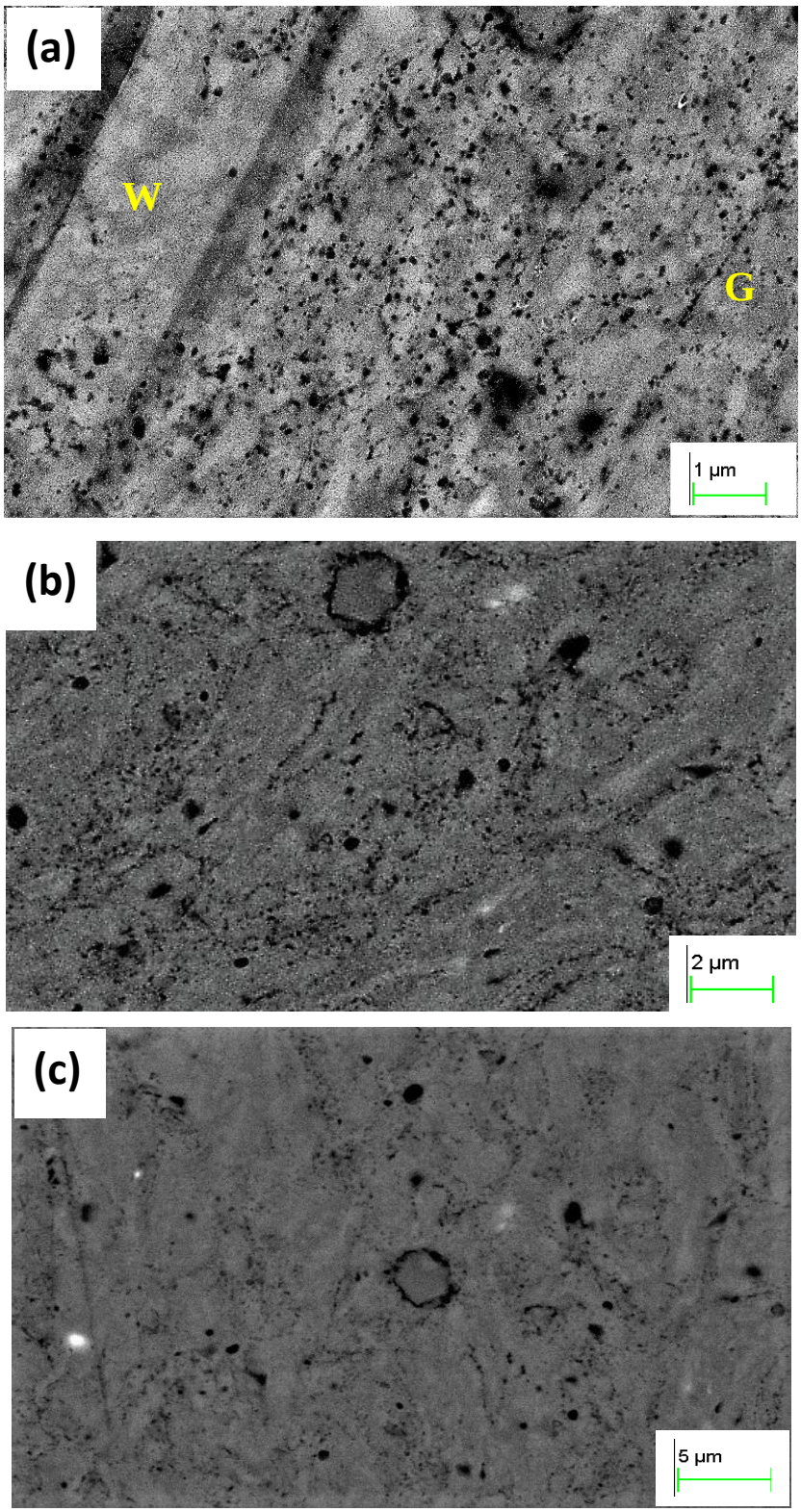

Fig 5.15: (a, b, c) Back scattered images of 4hr cryotreated TiAlNiCrFe sample.

Figure 5.16 below gives the elemental distribution (EDS Mapping) in 4hr cryotreated TiAlNiCrFe. All the elements are uniformly distributed in the matrix.

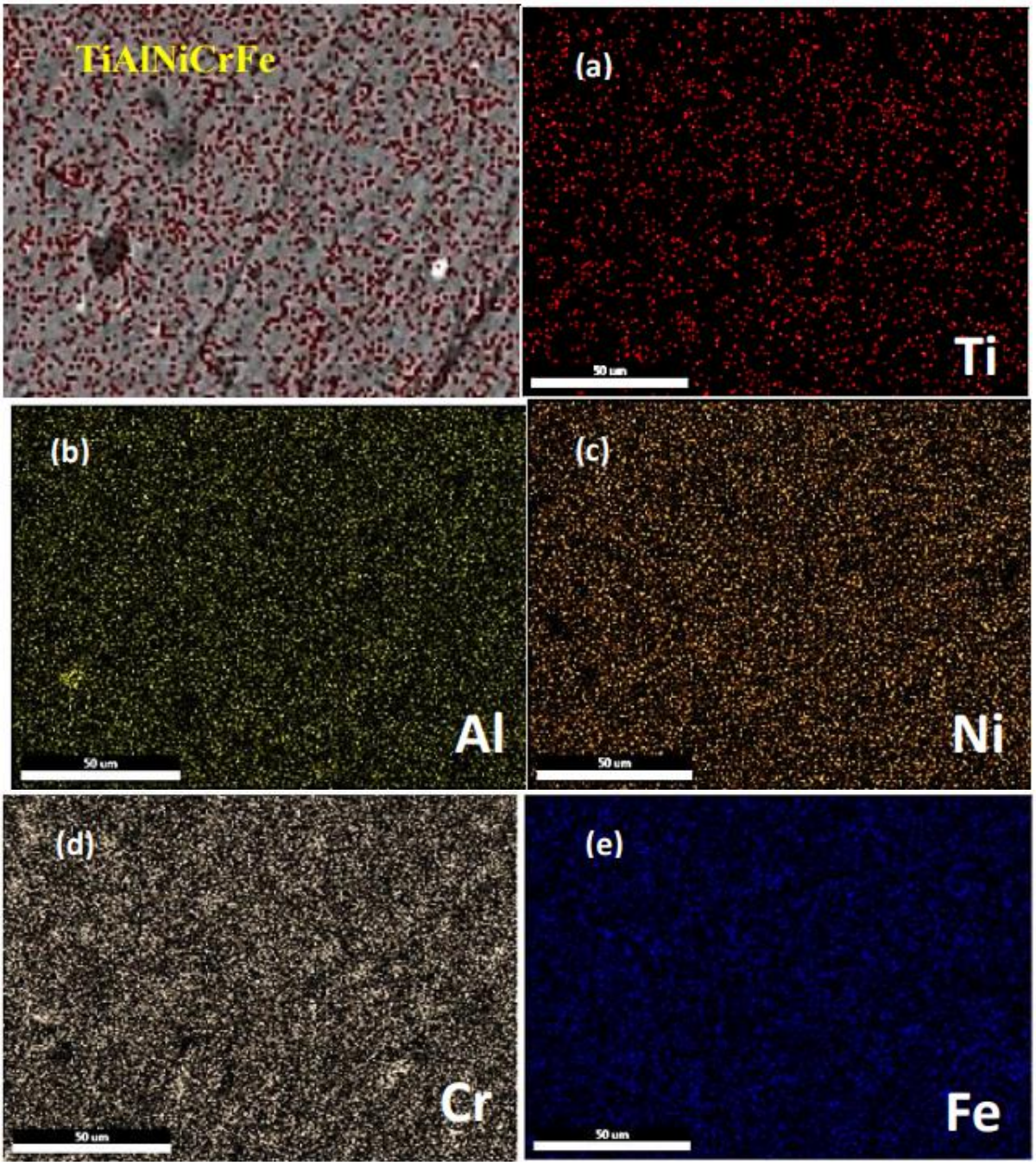

Fig 5.16: (a-e) EDS elemental mapping of 4hr cryotreated TiAlNiCrFe.

- 8hours treated TiAlNiCrFe sample 2.

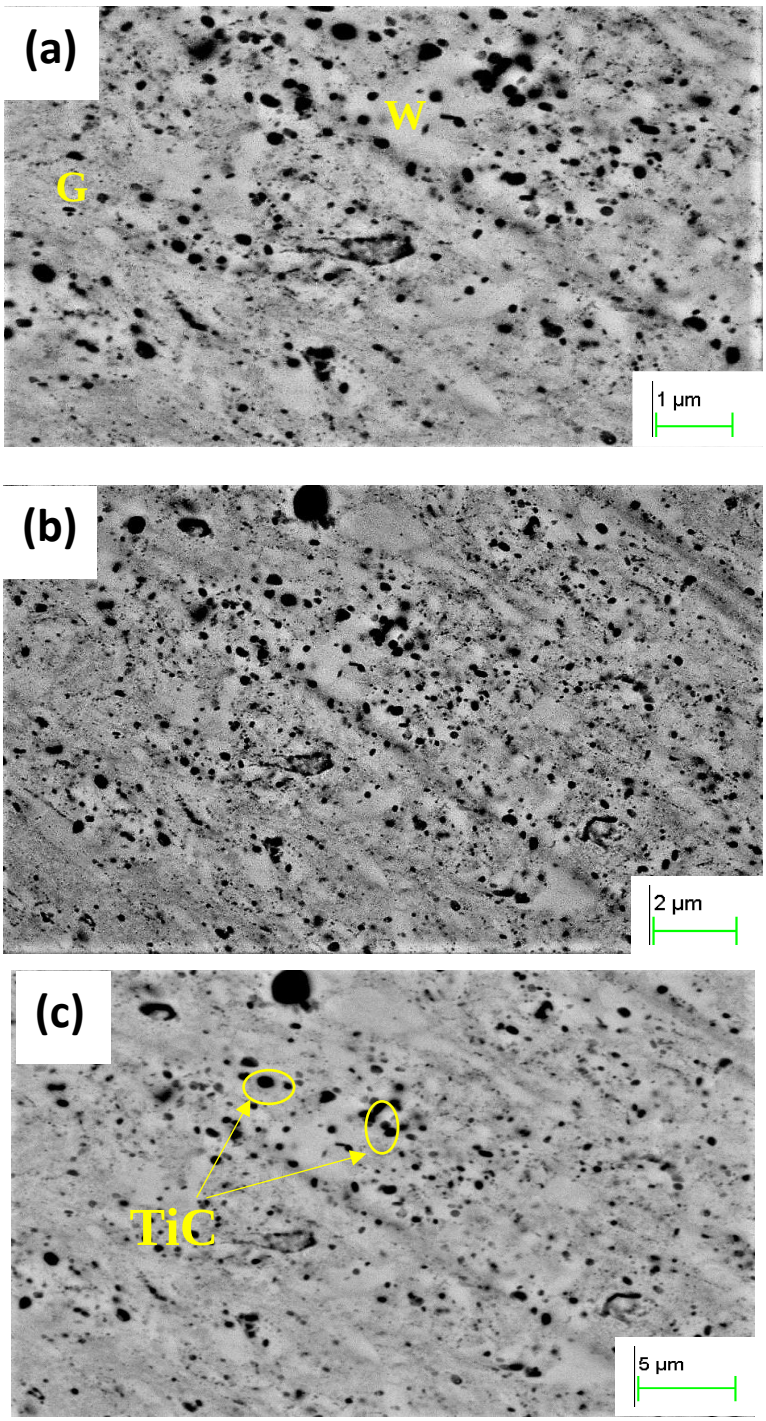

Fig 5.17: (a-c) Back scattered images of 8hr cryotreated TiAlNiCrFe sample.

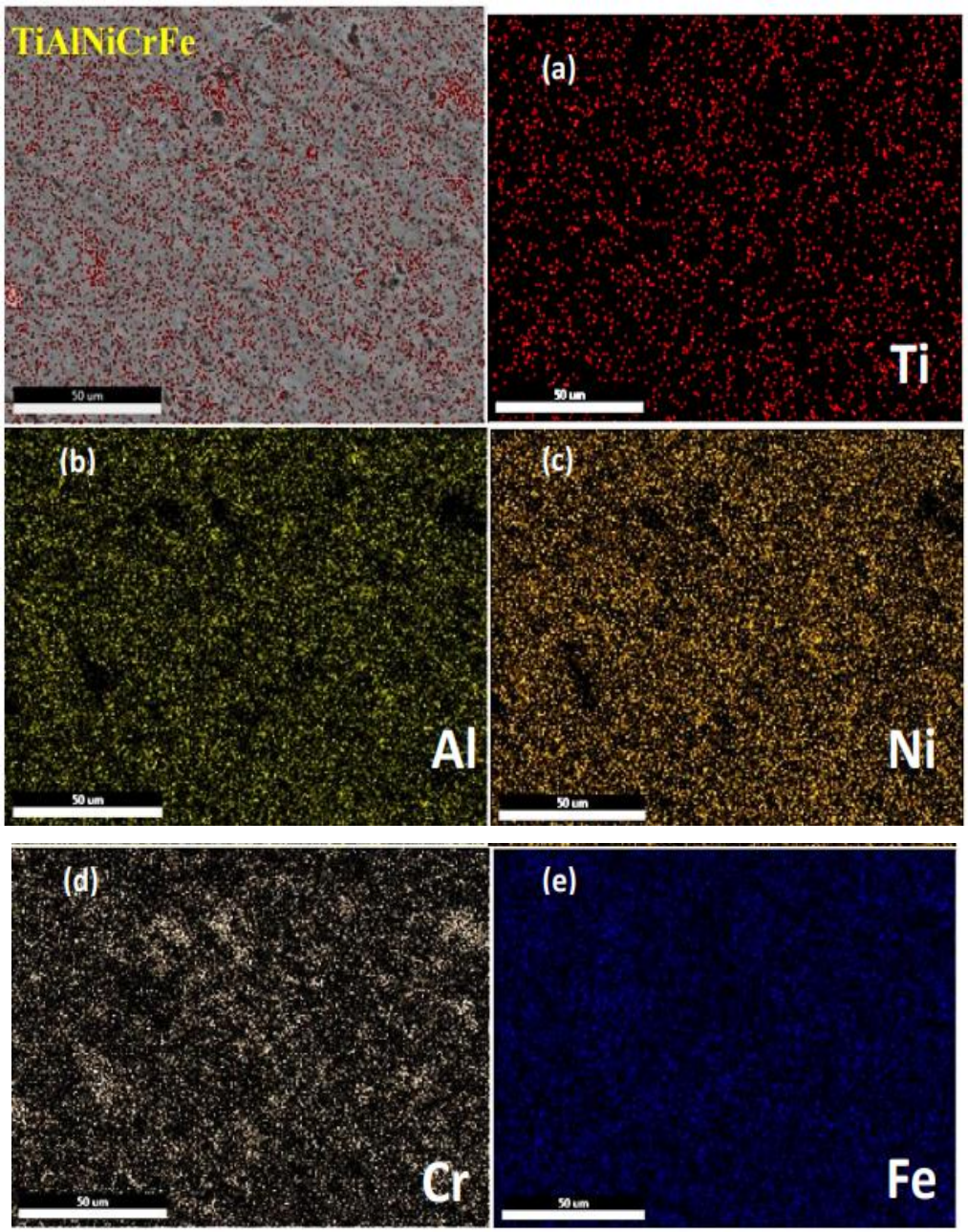

Fig 5.18: (a-e) EDS elemental mapping of 8hr cryotreated TiAlNiCrFe.

Figure 5.17 is the back scattered images of 8 hour cryotreated TiAlNiCrFe, also the elements are uniformly distributed. The matrix contains black dot particles that represent the SPS-derived contaminant TiC. The size of the TiC in the BSE image is larger than 4hr treated sample and here TiNi3 is also present. From the EDS analysis it is clear that the BCC structures are formed by Ni-Al, Cr-Fe element combinations.

The elemental distribution of selected area is mapped by EDS elemental mapping and shown in figure 5.18 (a-e) above. It shows that the whole elements are more closely arranged after 4hr and 8hr treated samples as compared to the EDS element mapping results figure.5.18(a-e).

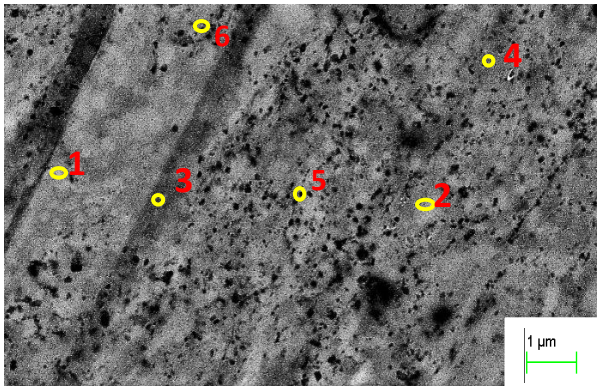

Fig 5.19: EDS Spot Analysis of TiAlNiCrFe specimen after 4hr CT.

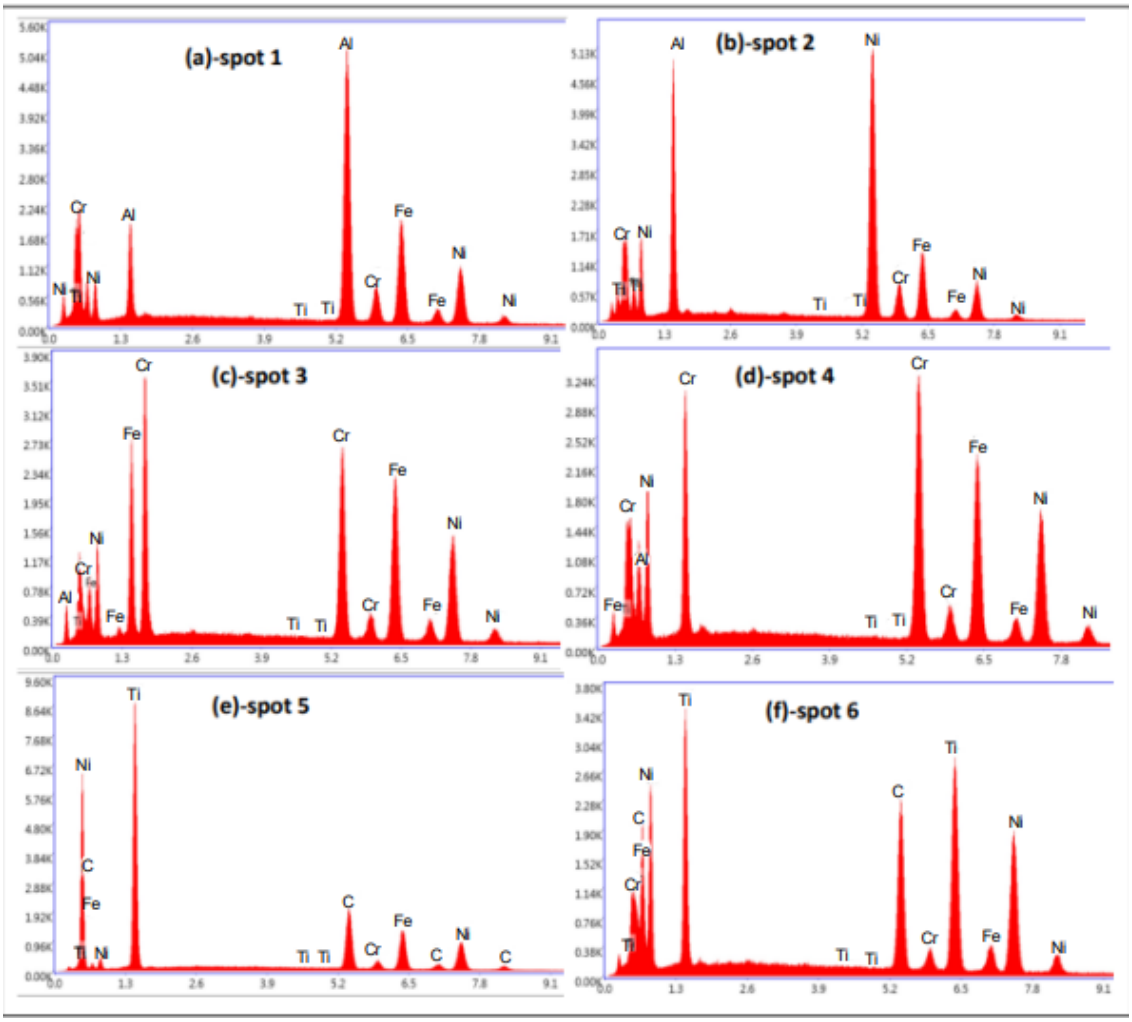

Fig 5.20: (a-f): Graph of EDS Analysis of TiAlNiCrFe 4hr cryotreated alloy

Table 5.8: EDS spot analysis composition (average) of elements in TiAlNiCrFe after 4hr treatment.

Elements	W region (spot1,2)	G region (spot3,4)	Black spot region (spot 5,6)
Ti	2.3	-	31.33
Al	41	7.39	14.23
Ni	33.4	23.05	15.18
Cr	16.1	40.36	13.72
Fe	7.2	29.2	9.33
C	-	-	16.21

From the spot analysis graph table (5.8), we can see that in white region the at% of Ni, Al is high which indicates that the white region forms Ni-Al BCC1 phases more in accordance with the XRD data also. Similarly, in the gray region (spot 3,4) the average percentage of Cr, Fe is increased as compared to before treatment table. This reveals that the gray region forms Cr-Fe BCC phase after 4hr treated TiAlNiCrFe. Black spots are same as compared to the nontreated samples.

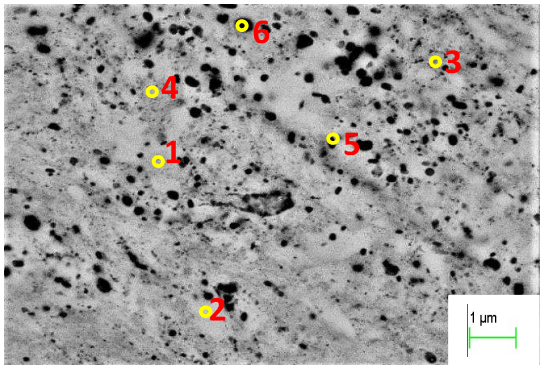

Fig 5.21: EDS Spot Analysis of TiAlNiCrFe specimen after 8hr CT.

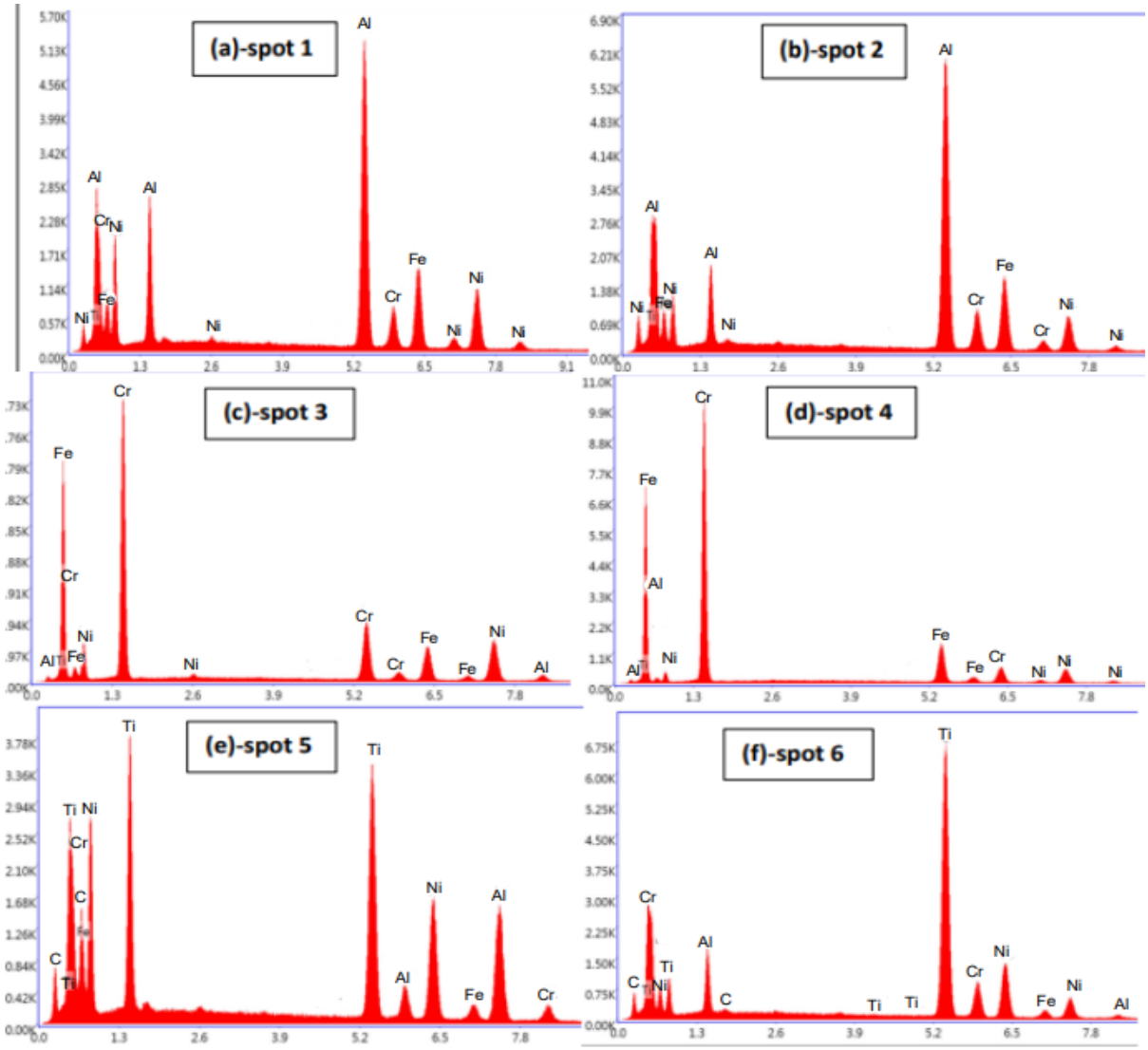

Fig 5.22:(a-f): Graph of EDS Analysis of TiAlNiCrFe 8hr cryotreated alloy.

Table 5.9: EDS spot analysis composition (average) of elements in TiAlNiCrFe after 8hr treatment.

Elements	W region (Spot 1,2)	G region (spot 2,3)	Black spots (spot5,6)
Ti	**-**	**-**	**34.22**
Al	**51.32**	**11.70**	**16.03**
Ni	**34.79**	**14.32**	**19.21**
Cr	**9.38**	**43.71**	**11.17**
Fe	**5.51**	**36.11**	**2.93**
C	**-**	**-**	**16.44**

From the EDS spot analysis, we get the elemental composition percentage in selected spots (6 spots), and the average element percentage is shown above table 5.9. There is not much variation in the at% of elements on spots after 8hr treatments.

Table 5.10: EDS elemental area mapping analysis composition (average) of elements in TiAlNiCrFe after 4hr,8hr treatment.

Element	4hr (at%)	8hr (at%)
Ti	**8.22**	**12.33**
Al	**26.32**	**28.60**
Ni	**28.24**	**27.40**
Cr	**26.54**	**21.67**
Fe	**10.68**	**10.0**

Compare to the percentage of elements before cryotreatment (table.5.3) the percentage of Cr is increased in different spots (4-hour treated sample). which also suggest that the formation of BCC Cr-Fe phase. Spot analysis on 8hours treated samples gives more percentage of Ti, Al in some spots which resembles the formation of TiNi3, also get it from XRD analysis (5.11) of 8-hour treated sample.

➢ 4hours treated TiAlNiCrCo sample 3.

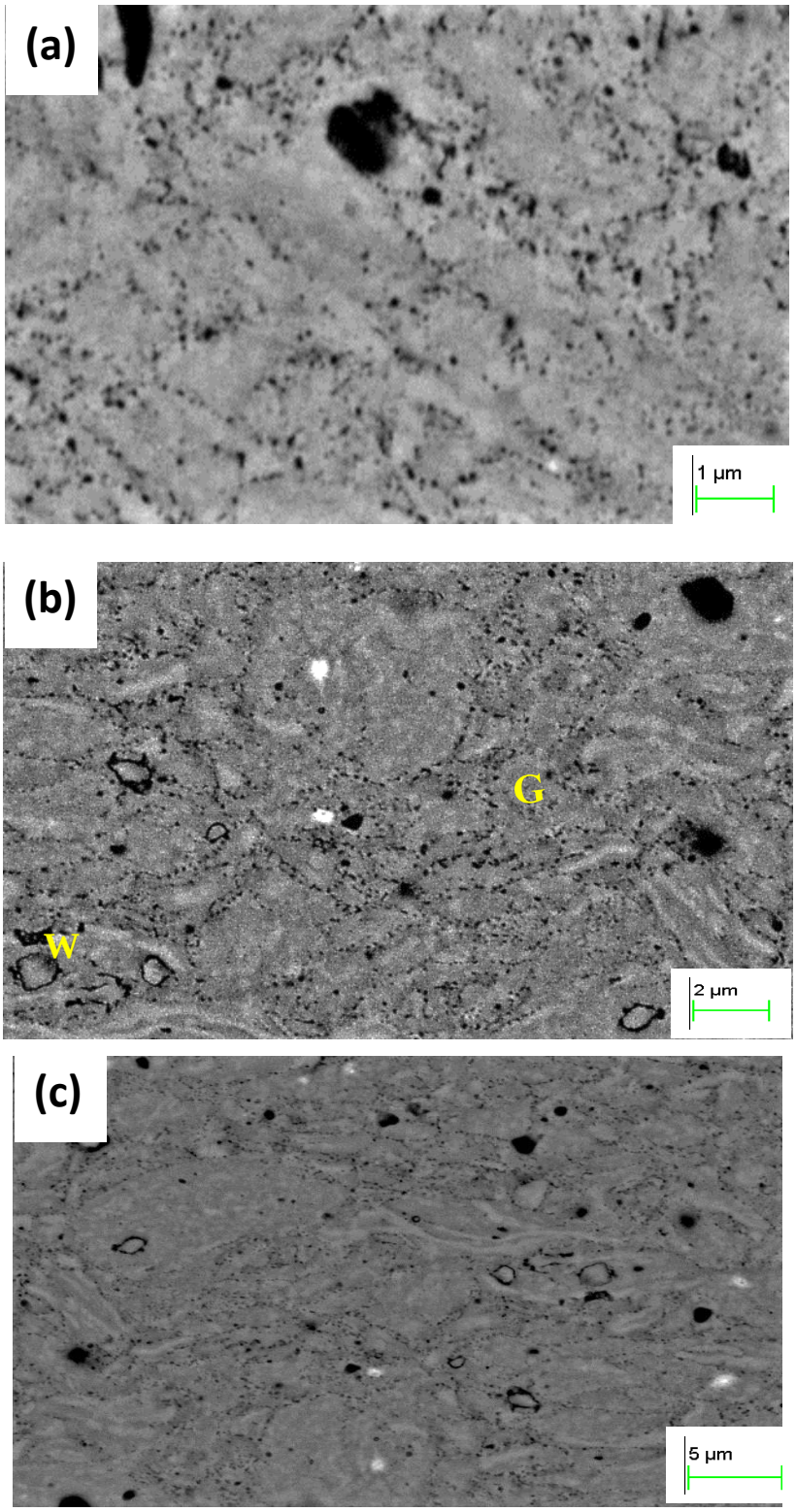

Fig 5.23: (a-c) Back scattered images of 4hr cryotreated TiAlNiCrCo sample

Similar to the as-sintered sample, 4-hour treated sample shows two major BCC phases denoted by white (W) and gray (G) regions. Fig. 5.23 shows the back scattered electroscope (BSE) images of 4-hour treated alloy, from this BSE images, the main BCC1(B2) and BCC are clearly visible and black dots represents the presence of TiC particles.

Figure 5.24 gives the EDS mapping which gives the elemental distribution. After the 4-hour treatment the samples shows more closed distributions. Thus, may increase the strength of the samples.

The elemental distribution of selected area is mapped by EDS elemental mapping and shown in figure 5.24 (a-e) below.

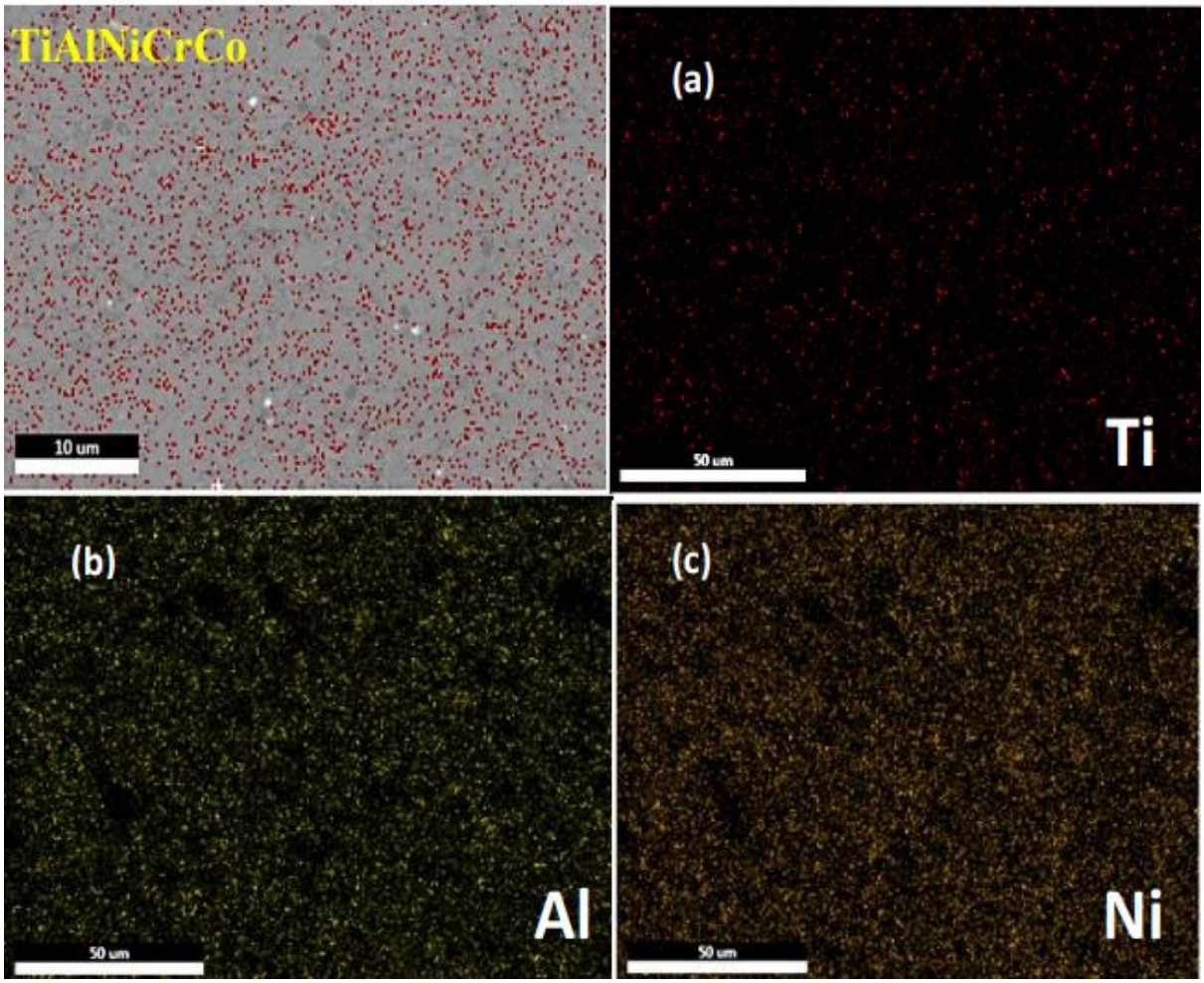

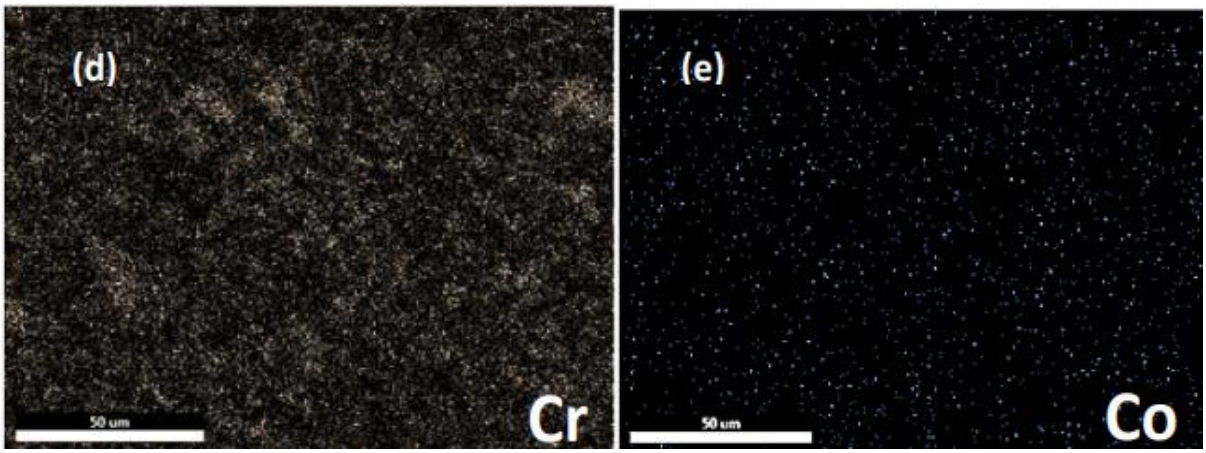

Fig 5.24: (a-e) EDS elemental mapping of 4hr cryotreated TiAlNiCrCo.

- 8hours treated TiAlNiCrCo sample 4.

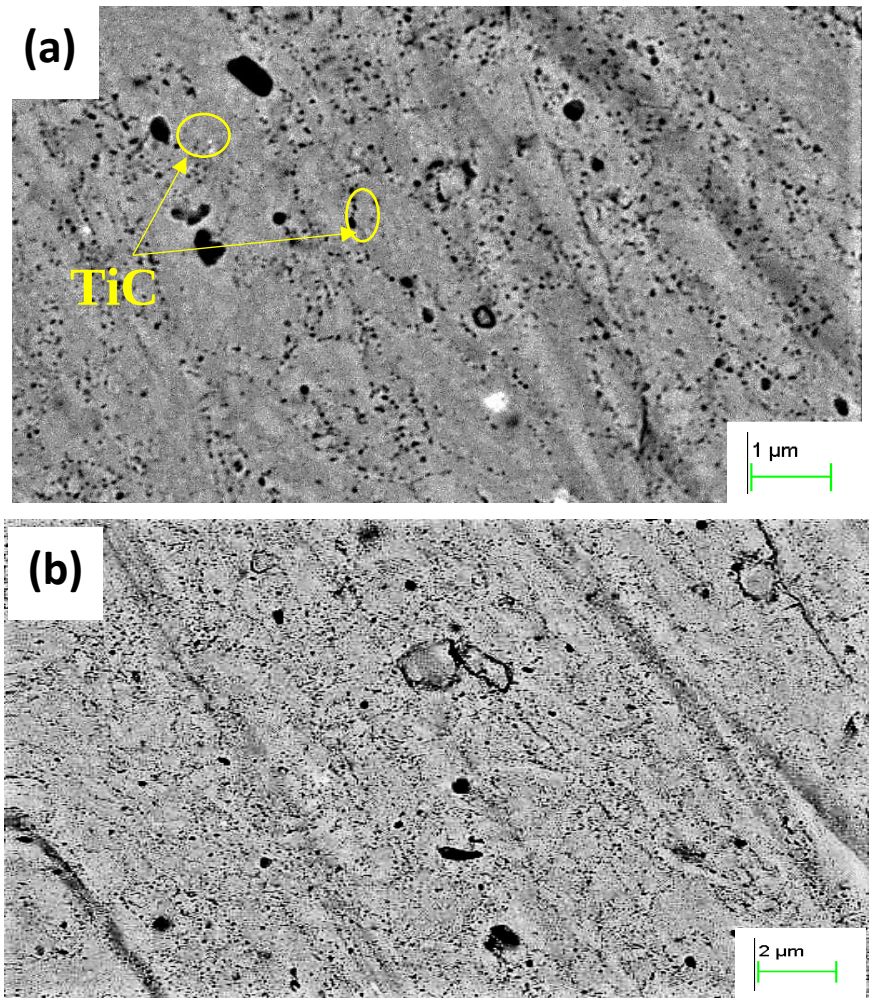

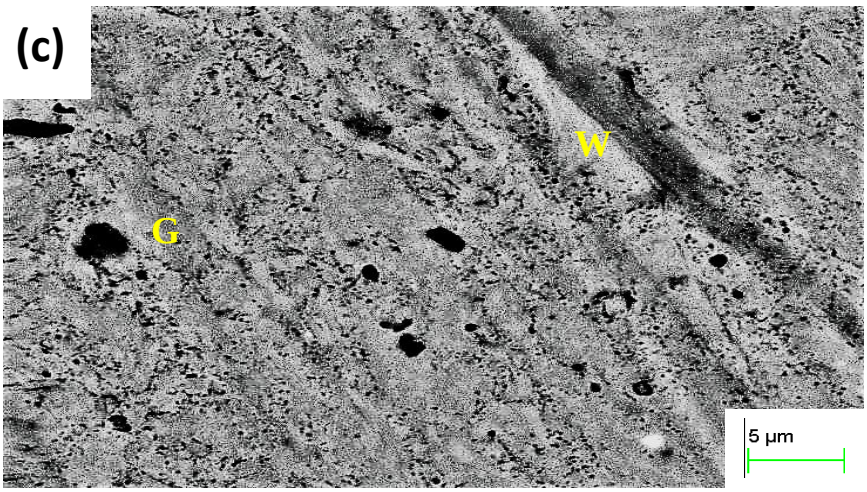

Fig 5.25: (a, b, c) Back scattered images of 8hr cryotreated TiAlNiCrCo sample.

The BSE images of 8-hour treated TiAlNiCrCo sample is shown above (fig. 5.25). Comparing BSE images of nontreated TiAlNiCrCo samples, fig.5.23 shows the elements are finely distributed and the white, gray regions boundaries are not much clear. The elemental composition and its distribution were analyzed by using EDS and figure 5.26(a-e) is the EDS mapping of sample.

The white (W) and gray (G) region is not clearly visible in this alloy. Similar to TiAlNiCrCo alloy, it forms two BCC phases. Connecting with the XRD peaks and EDS spot, the BCC1(B2) peaks correspond to Ni-Al, while the BCC2 phase contains Cr-Fe. Black spots represent TiC, TiNi3 agglomerations.

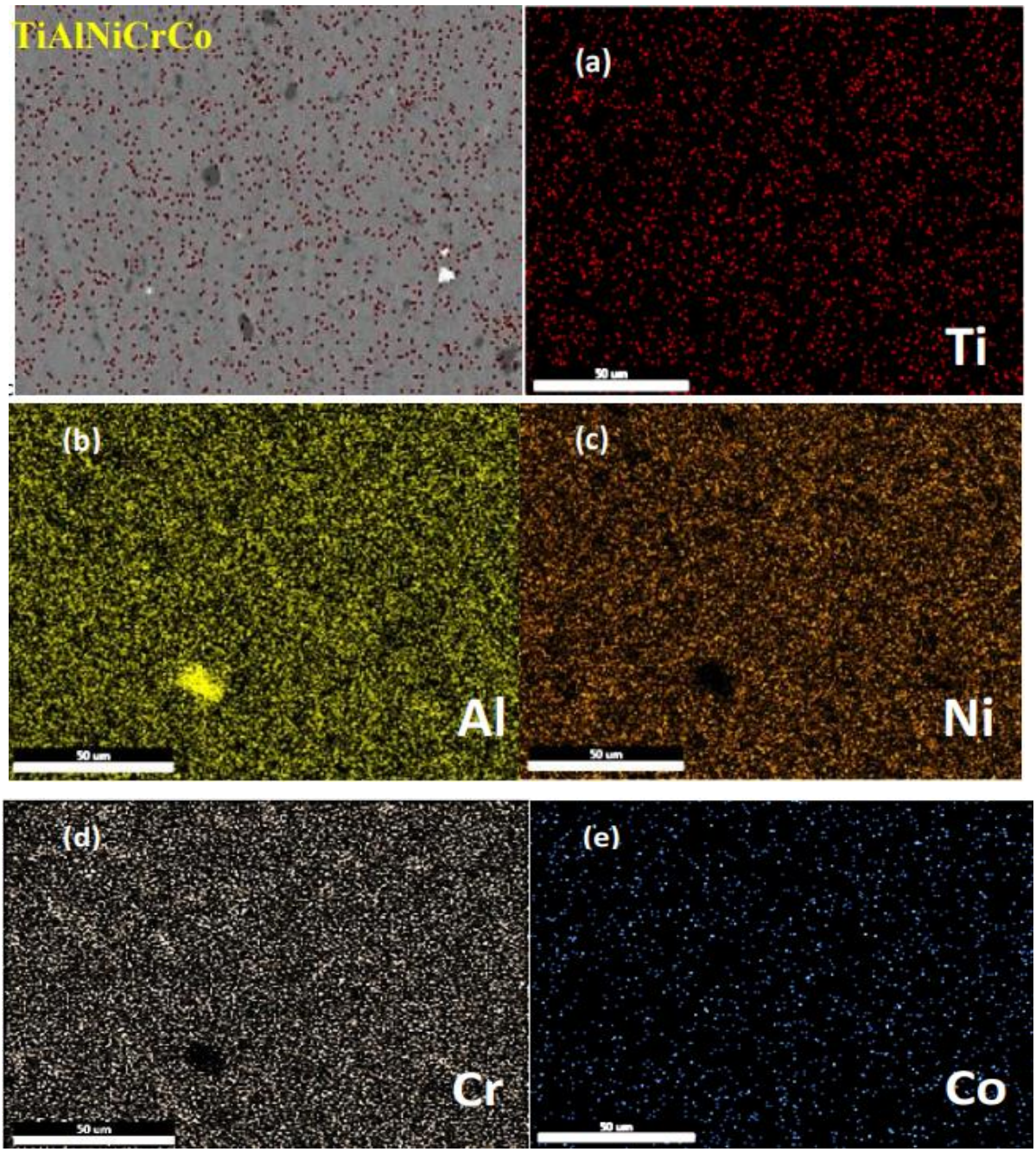

Fig 5.26: (a-e) EDS elemental mapping of 8hr cryotreated TiAlNiCrCo

Table 5.11: EDS area mapping analysis- composition (average) of elements in TiAlNiCrCo after 4hr,8hr treatment.

Element	4hr (at%)	8hr (at%)
Ti	**9.42**	**9.19**
Al	**27.33**	**29.33**
Ni	**26.82**	**26.21**
Cr	**28.10**	**25.30**
Co	**8.33**	**9.97**

There is no change in composition of elements. Compare to the percentage of elements before cryotreatment (table.5.3) the percentage of Al and Ni are increased in different spots (4-hour and 8-hour treated samples). Which also suggest that the formation of BCC1 Ni-Al phase connect with XRD data. Spot analysis on 8hours treated samples gives more percentage of Co than 4-hour treated sample.

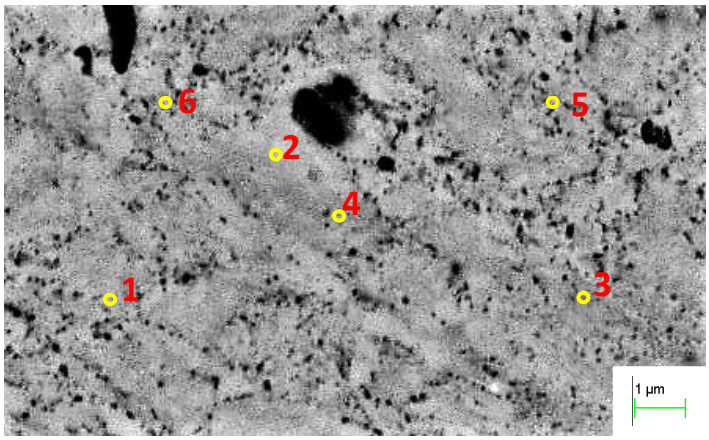

Fig 5.27: EDS Spot Analysis of TiAlNiCrCo specimen after 4hr CT.

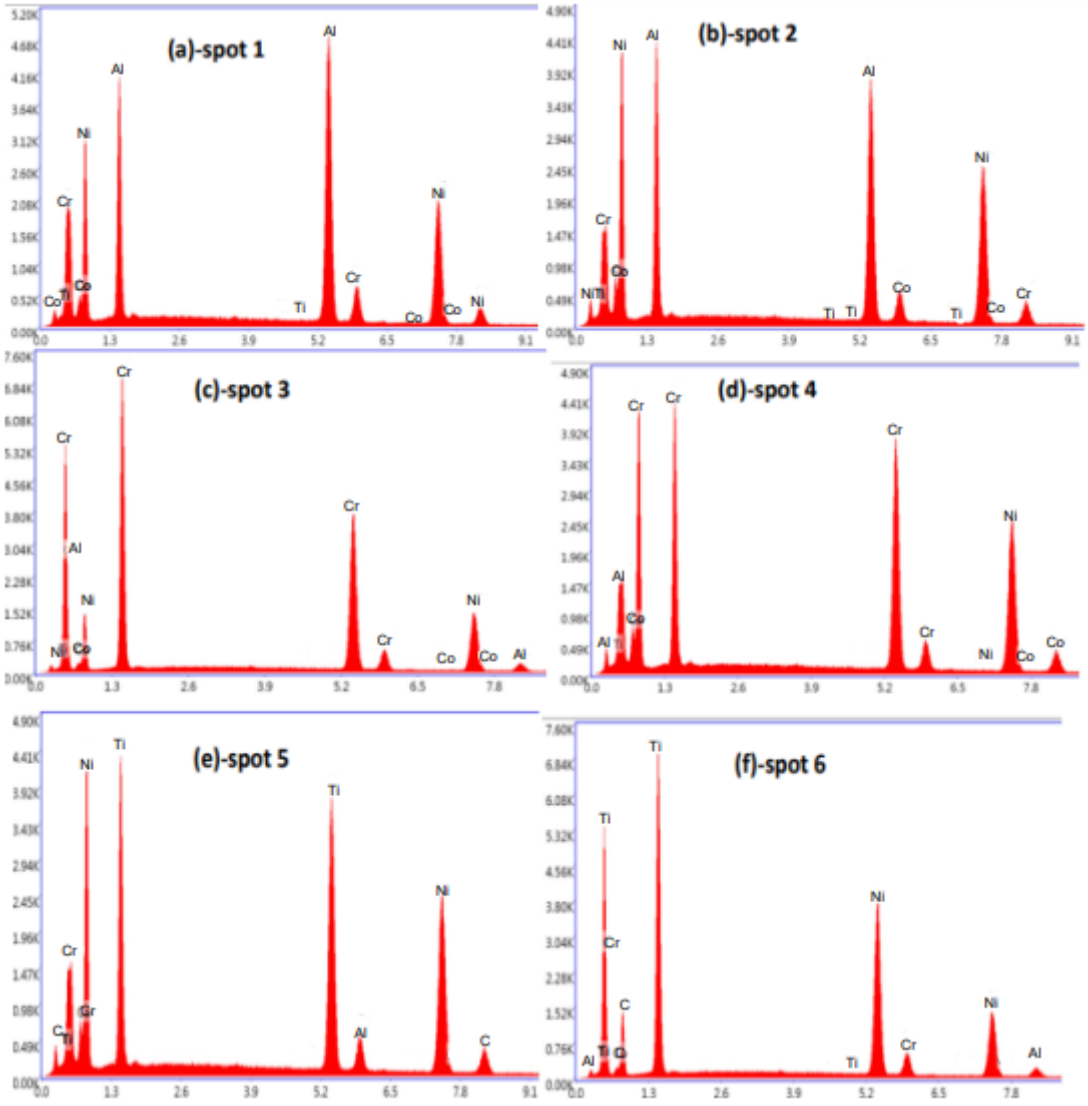

Fig 5.28.(a-f): Graph of EDS spot analysis of TiAlNiCrCo 4hr cryotreated alloy.

Table 5.12: EDS spot analysis composition (average) of elements in TiAlNiCrCo after 4hr treatment.

Elements	W region (Spot 1,2-at%)	G region (Spot 3,4-at%)	Black spots (Spot-5,6 at%)
Ti	2.31	-	35.21
Al	44.24	18.33	16.33
Ni	31.34	12.41	17.11
Cr	13.11	62.31	14.38
Co	9.0	6.95	-
C	-	-	16.97

From the spot analysis graph table, we can see that in white region the at% of Ni, Al is high which indicates that the white region forms Ni-Al BCC1(B2) phases more in accordance with the XRD data also. Similarly, in the gray region (spot 3,4) the average percentage of Cr, is not changed as compared to before treatment table. This reveals that the gray region forms Cr alone BCC phases after 4hr treated TiAlNiCrCo. Black spots are same as compared to the nontreated samples.

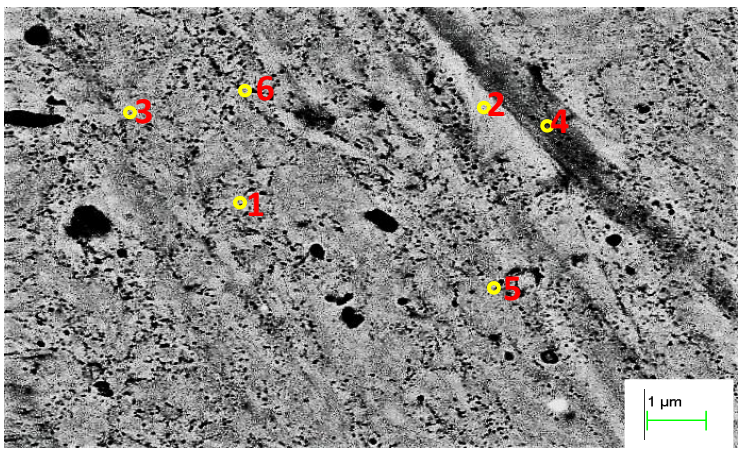

Fig 5.29: EDS Spot Analysis of TiAlNiCrCo specimen after 8hr CT.

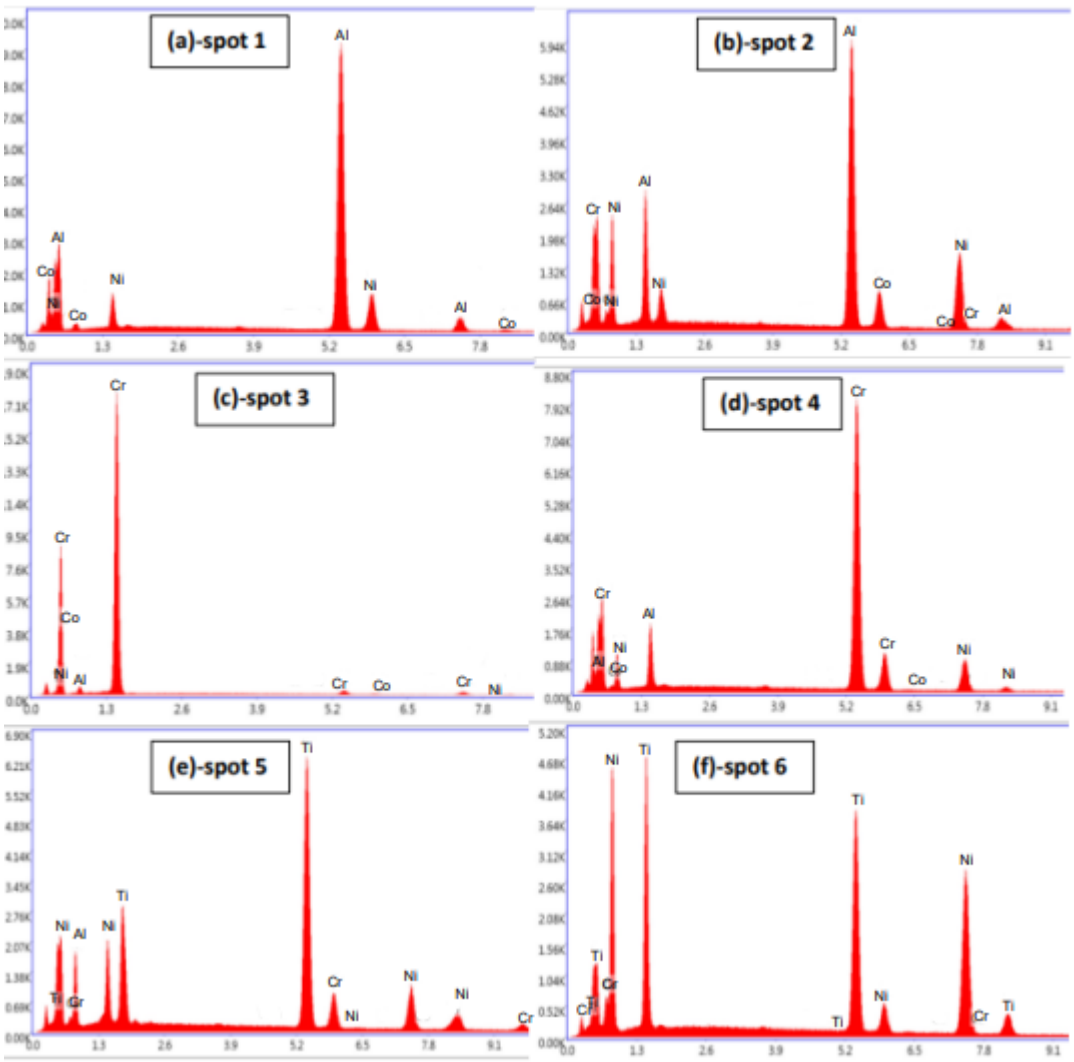

Fig 5.30.(a-f): Graph of EDS spot analysis of TiAlNiCrCo 8hr cryotreated alloy.

Figure 5.30(a-f) is the EDS spot analysis graph. From the EDS spot analysis, we get the elemental composition percentage of selected spots (6 spot), and the average element percentage is shown table 5.13.

Table 5.13: EDS spot analysis composition (average) of elements in TiAlNiCrCo after 8hr treatment

Elements	W region (Spot 1,2-at%)	G region (Spot 3,4-at%)	Black spots (Spot-5,6 at%)
Ti	**-**	**-**	**33.01**
Al	**47.08**	**22.28**	**16.21**
Ni	**31.91**	**13.28**	**19.22**
Cr	**11.01**	**51.03**	**12.36**
Co	**10.0**	**13.41**	**-**
C	**-**	**-**	**19.20**

From the spot analysis graph table, we can see that in white region (spot 1,2) the at% of Ni, Al is high which indicates that the white region forms Ni-Al BCC1 phases more in accordance with the XRD data also. Similarly, in the gray region (spot 3,4) the average percentage of Cr, is decreased as compared to 4hr treatment table and Co percentage is increased in both white and gray regions. Black spots are same as compared to the nontreated samples and Ni content is slightly increased.

5.2.3 MECHANICAL PROPERTIES

The hardness of the cryotreated alloys is displayed in Table 5.14. According to this table, both alloys hardness values first increased and then decreased.

The samples treated for four hours are shown by the maximum hardness value. For TiAlNiCrFe the hardness value is increased 11.25% from 755 HV to 840 HV. Alloys hardness was increased due to the reduction in crystallite size and TiC, TiNi3 agglomerations. Deep cryogenic treatment enhanced the alloy's deformation resistance and hardness by strengthening its microstructure, which resulted in fine crystals. Alloy hardness reduced when deep cryogenic treatment lasted more than 4-hour. The BCC phases (Ni-Al, Cr-Fe) and the TiC dispersions are responsible for the alloys increased strength and hardness.

For TiAlNiCrCo samples, the hardness value for 4h treated is increased from 702 HV to 758 HV, and for 8-hour treated alloy that hardness is less increased because of the formation of increase in crystallite sizes.

Table 5.14: Hardness values of samples before and after cryotreatment.

SAMPLE	HARDNESS VALUE (HV) (BEFORE CT)	4 HR. TREATED SAMPLE(HV)	8 HR. TREATED SAMPLE (HV)
TiAlNiCrFe	**755 ± 8 HV**	**840 ± 3 HV**	**794 ± 6**
TiAlNiCrCo	**702 ± 6 HV**	**758± 5 HV**	**728 ± 7**

CHAPTER 6
CONCLUSIONS

Multicomponent alloys of TiAlNiCrFe and TiAlNiCrCo were effectively created through the ball milling of elemental powders and Spark Plasma Sintering. XRD patterns showed that both materials had substantial two-BCC phases after Spark plasma sintering. In TiAlNiCrFe and TiAlNiCrCo samples, SEM BSE images of the microstructure samples showed a fine dispersion of the two BCC phases coupled with a fine dispersion of TiC nanoparticles. The distribution of the elements is more or less consistent across all of the alloys, according to the elemental compositions that were examined using EDS at distinct areas (spot analysis). From the EDS analysis, the BCC1(B2) phase was identified as a Ni-Al-rich phase, and the BCC2 phase was identified as a Cr/CrFe-rich phase (a CrFe-rich phase for TiAlNiCrFe alloy and a Cr-alone phase for TiAlNiCrCo alloy).

The impact of deep cryogenic treatment on the phase composition, microstructure, and mechanical characteristics of TiAlNiCrFe and TiAlNiCrCo high-entropy alloys was then investigated. The XRD patterns say that the 4 and 8-hour treated TiAlNiCrFe and TiAlNiCrCo samples show major BCC peaks similar to as-sintered alloys, except that small TiNi3 peaks are also present in both 4, 8-hour treated alloys. From the XRD peak with W-H plot analysis we can understand that the cryotreatment process reduce the crystallite size of both HEAs samples. Crystallite size is finer at 4 hour treated samples. SEM BSE images reveal that 4-hour treated alloys have a more uniformly dispersed matrix than 8-hour treated alloys, and 8-hour treated alloys show some elemental agglomerations. The EDS spot analysis on six different spots suggests that the 4,8-hour cryotreated alloys show Ni-Al-rich BCC1(B2) phases and Cr/Cr-Fe-rich BCC2 phases. Vickers indenter measurements of the alloys hardness also provide positive outcomes. Hardness seemed to rise initially before decreasing as the duration of the cryogenic treatment increased. At 4-hour treated samples, the maximum hardness was attained, that is hardness value is increased with decrease in crystallite size. The hardness value of TiAlNiCrFe alloy after 4-hour treatment rises from 755 HV to 840 HV by 11.25%.

REFERENCES

[1] B. Cantor, I.T.H. Chang, P. Knight, A.J.B. Vincent (2004), Microstructural development in equiatomic multicomponent alloys, *Materials Science and Engineering*, A 375–377, 213–218.

[2] Chengze Li, Yingdong Qu, Yufeng Zhang (2020), Effect of deep cryogenic treatment on the microstructure and mechanical properties of AlCrFe2Ni2 High-entropy alloy, *Mater. Res. Express* 7 (2) 036504

[3] Vikas Kukshal, Amar Patnaik, I.K. Bhat (2018), Effect of cobalt on microstructure and properties of AlCr1.5CuFeNi2 Cox high-entropy alloys, *Materials Research Express*, Volume -5, No-6

[4] M. Klimova, D. Shaysultanov, A. Semenyuk (2020), Effect of nitrogen on mechanical properties of CoCrFeMnNi high entropy alloy at room and cryogenic temperatures, *Journal of Alloys and Compounds*, 849 (2) 156633.

[5] Wujing Fu, Wei Zheng, Yongjiang Huang (2020), Cryogenic mechanical behaviors of CrMnFeCoNi high-entropy alloy, *Materials Science & Engineering* A, 789 -139579.

[6] Daniel Costas Bosque (2018), Study of the addition of aluminum to the high entropy system HfMoTaTi+Al, *Material Science & Engineering*, T7009

[7] W.H. Liu a, H. Wang a, Y. Wu a, X.J. Liu (2014), Effects of Al addition on structural evolution and tensile properties of the FeCoNiCrMn high-entropy alloy system, *Acta Material* 62, 105–113.

[8] Anand Sekhar R, Sumanta Samal, Niraj Nayan (2019), Microstructure and mechanical properties of Ti-Al-Ni-Co-Fe based high entropy alloys prepared by powder metallurgy route, *Journal of Alloys and Compounds*, 787, 123-132.

[9] Sajid Ali Alvi (2019), Synthesis and Characterization of High Entropy Alloy and Coating, *Engineering Materials*, 1402-1757.

[10] Amanendra Kushwaha et al. (2019), Influence of Cryomilling on Crystallite Size of Aluminium Powder and Spark Plasma Sintered Component, *Nanomaterials*,12(3):551.

[11] Liyang Fanga, Jun Wanga, Xiaoning Li (2022), Effect of Cr content on microstructure characteristics and mechanical properties of ZrNbTaHf0.2Crx refractory high entropy alloy, *Journal of Alloys and Compounds*, 92-16593.

[12] Chun-mei Li, Nan-pu Cheng1, Zhi-qian Chen (2015), Deep-cryogenic-treatment-induced phase transformation in the Al–Zn–Mg–Cu alloy, *International Journal of Minerals, Metallurgy and Materials* Volume 22-Page 68

[13] Srinivasa Rao Bakshi, R. Anand Sekhar (2019), Microstructural Evolution of Ti–Al–Ni (Cr, Co, Fe)-Based High-Entropy Alloys Processed Through Mechanical Alloying, *Trans Indian Inst Met*, -019-01596.

[14] Zhiyi Ronga, Chaohui Wanga, You Wang (2022), Microstructure and properties of FeCoNiCrX (X]Mn, Al) high-entropy alloy coatings, *Journal of Alloys and Compounds*, 921-1660.

[15] R. Sriharitha, B.S. Murty, Ravi S. Kottada (2014), Alloying, thermal stability and strengthening in spark plasma sintered AlxCoCrCuFeNi high entropy alloys, *Journal of Alloys and Compounds*,583, 419–426.

[16] S. Varalakshmi, M. Kamaraj, B.S. Murty (2010), Processing and properties of nanocrystalline CuNiCoZnAlTi high entropy alloys by mechanical alloying, *Materials Science and Engineering A*,527, 1027–1030.

[17] Guocai Chai (2007), Spark plasma sintering and deformation behavior of Titanium and Titanium/TiB2 composites, *Mirva Eriksson Licentiate Thesis Division of Inorganic Chemistry*.

[18] Y.F. Ye, Q. Wang, J. Lu, C.T. Liu and Y. Yang (2016), High-entropy alloy: challenges and prospects, *Materials Today*, Volume 19

[19] P. Karuppusamy, K. Lingadurai and V. Sivananth (2019), Influence of Cryogenic Treatment on As-Cast AZ91+1.5 wt%WC Mg-MMNC Wear Performance, *Advances in Materials and Metallurgy*, 13-1780-419.

[20] R. Anand Sekhar, Srinivasa Rao Bakshi (2019), Microstructure and Mechanical Properties of Ti–Al–Ni–Cr–Co– Fe-Based High-Entropy Alloys, *Trans Indian Inst Met*,1413-1416.

[21] Zhiming Guo, Aijun Zhang, Jiesheng Han (2018), Effect of Si additions on microstructure and mechanical properties of refractory NbTaWMo high-entropy alloys, *J Mater Sci*, 10853-018-03280.

[22] Yong Zhang (2019), Preparation Methods of High-Entropy Materials, *High-Entropy Materials. Springer*, 65–75, 13-8525-4.

[23] K. Vasanthakumar, Srinivasa Rao Bakshi (2017), Effect of C/Ti ratio on densification, microstructure and mechanical properties of TiCx prepared by reactive spark plasma sintering, *Ceramics International*, 484-494.

[24] Zhangwei Wang, Ian Baker, Zhonghou Cai (2016), The effect of interstitial carbon on the mechanical properties and dislocation substructure evolution in Fe40.4Ni11.3Mn34.8Al7.5Cr6 high entropy alloys, *Acta Materialia*, 120, 228-239.

[25] Xiaodong Sun, Heguo Zhu, Jianliang Li (2018), High entropy alloy FeCoNiCu matrix composites reinforced with in-situ TiC particles and graphite whiskers, *Materials Chemistry and Physics*,30773-9.

[26] C.D. Gómez-Esparza, J. Camarillo-Cisneros, I. Estrada-Guel (2014), Effect of Cr, Mo and Ti on the microstructure and Vickers hardness of multicomponent systems, *Journal of Alloys and Compounds*, 00112-1.

[27] Minju Kang, Ka Ram Lim, Jong Woo Won, Young Sang Na (2018), Effect of Co content on the mechanical properties of A2 and B2 phases in AlCoxCrFeNi high-entropy alloys, *Journal of Alloys and Compounds*, 925-8388.

[28] J. Cieslak, J. Tobola (2018), Phase composition of AlxFeNiCrCo high entropy alloys prepared by sintering and arc-melting methods, *Journal of Alloys and Compounds*, 264-272.

[29] Y.Y. Chen, T. Duval, U.D. Hung, J.W. Yeh, H.C. Shih (2005), Microstructure and electrochemical properties of high entropy alloys—a comparison with type-304 stainless steel, *Corrosion Science* 47,2257–2279.

[30] S. Varalakshmi, M. Kamaraj, B.S. Murty (2008), Synthesis and characterization of nanocrystalline AlFeTiCrZnCu high entropy solid solution by mechanical alloying, *Journal of Alloys and Compounds* 460,253–257.

[31] Kyung-Hwan Jung, Minh Tien Tran, Zhengtong Shan (2023), Correlation of cryogenic deformation mechanisms to excellent strength-ductility of CrCoNi medium entropy alloy processed by selective laser melting, *Journal of Materials Research and Technology*,97- [315.

[32] Yuze Wu, Zhaoyang Zhang, Yun Zhang (2022), Twinning susceptibility of CrCoNi medium entropy alloy to cryogenic temperature during asymmetric rolling, *Journal of Materials Research and Technology* 638-649.

[33] Joshua A. Smeltzer, Mari-Therese Burton, B. Chad Hornbuckle (2021), Optimization of cryogenic mechanical alloying parameters to synthesize ultrahard refractory high entropy materials, *Materials & Design*, 210 – 110070.

[34] Huang, Zhao et al. (2022), Overcoming the strength ductility trade off in an additively manufactured CoCrFeMnNi high entropy alloy via deep cryogenic treatment, *Additive Manufacturing,* Vol 50 (102546).

[35] Hongge Li, Tian Chen et al. (2023), Beneficial effects of deep cryogenic treatment on mechanical properties of additively manufactured high entropy alloy: cyclic vs single cryogenic milling, *Journal of Materials Science & Technology,* Vol (115),40-51.

[36] Patricia Jovicevic-Klung et al. (2022), Coupled role of alloying and manufacturing on deep cryogenic treatment performance on high alloyed ferrous alloys, *Journal of Materials Research and Technology,* Vol (18),3184-3197.

[37] Rahul Parmar, Matteo Amati et al. (2023), Understanding carbide evolution and surface chemistry during deep cryogenic treatment in high alloyed ferrous alloy, *Applied Surface Science,* Vol (610),155497.

[38] Xiaosong Jiang et al. (2022), Effect of deep cryogenic treatment on microstructure and mechanical properties of a CoCrFeNiMo medium-entropy alloy, *Materials Testing*,64(4):463-472.

[39] Luo Kaiguang et al. (2023), Mechanical properties and microstructure evolution of cryorolled AlCoCrFeNi reinforced aluminium matrix composite tensile tested at room and cryogenic temperature, *Metallurgical and Materials Transactions A*, Vol 54,2292-2310.

[40] Erfan Abbasi, Kamran Dehghani, (2019), Cryogenic treatment of CoCrFeMnNi (NbC) high entropy alloys, *Journal of Materials Engineering and Performance*,28(6201).

[41] Yali Zhang, Fang Luo et al. (2022), Effect of deep cryogenic treatment on microstructure and mechanical properties of a CoCrFeNiMo medium entropy alloy, *Material Testing* ,2021-2049.

[42] Gurkirat Singh et al. (2023), Effect of deep cryogenic treatment, tempering temperature and time on hardness of Nimnonic-90, *Journal of Process Mechanical Engineering*,2023;0(0).